Machine learning of hematopoietic stem cell divisions from paired daughter cell expression profiles reveals effects of aging on self-renewal

Fumio Arai[1,†,*], Patrick S. Stumpf[2,†], Yoshiko M. Ikushima[3,†], Kentaro Hosokawa[1], Aline Roch[4], Matthias P. Lutolf[4], Toshio Suda[5], and Ben D. MacArthur[2,6,7,* ††]

[1]Department of Stem Cell Biology and Medicine, Graduate School of Medical Sciences, Kyushu University, 812-8582, Fukuoka, Japan.
[2]Centre for Human Development, Stem Cells and Regeneration, University of Southampton, SO17 1BJ, UK
[3]Research Institute National Center for Global Health and Medicine, Tokyo, Japan
[4]Laboratory of Stem Cell Bioengineering, Institute of Bioengineering, School of Life Sciences and School of Engineering, Ecole Polytechnique Federale de Lausanne (EPFL), CH-1015 Lausanne, Switzerland
[5]Cancer Science Institute, National University of Singapore, 14 Medical Drive, MD6, 117599 Singapore, Singapore
[6]Institute for Life Sciences, University of Southampton, SO17 1BJ, United Kingdom
[7]Mathematical Sciences, University of Southampton, SO17 1BJ, United Kingdom
[*]Correspondence to Fumio Arai (farai@med.kyushu-u.ac.jp) and Ben MacArthur (bdm@soton.ac.uk)
[†]These authors contributed equally.
[††]Lead Author

ABSTRACT

Changes in stem cell activity may underpin aging. However, these changes are not completely understood. Here, we combined single cell profiling with machine learning and in vivo functional studies to explore how hematopoietic stem cell (HSC) divisions patterns evolve with age. We first trained an artificial neural network (ANN) to accurately identify cell types in the hematopoietic hierarchy and predict their age from single cell gene expression patterns. We then used this ANN to compare identities of daughter cells immediately after HSC divisions and found that the self-renewal ability of individual HSCs declines with age. Furthermore, while HSC cell divisions are deterministic and intrinsically regulated in young and old age, they are variable and niche-sensitive in mid-life. These results indicate that the balance between intrinsic and extrinsic regulation of stem cell activity alters substantially with age and help explain why stem cell numbers increase through life, yet regenerative potency declines.

HIGHLIGHTS

- Machine learning predicts cell identities and ages from gene expression patterns.
- The potency of individual hematopoietic stem cells (HSCs) declines with age.
- HSC divisions are maximally sensitive to niche instruction in mid-life.
- HSCs acquire aged characteristics from the first division when cultured ex vivo.

INTRODUCTION

Hematopoietic stem cells (HSCs) are able to give rise to all cell types in the hematopoietic lineages, and are responsible for ensuring healthy life-long hematopoiesis (Orkin & Zon 2008). To do so, they must regulate their own numbers and simultaneously produce differentiated progeny in precisely regulated proportions. Maintaining this balance requires HSCs to have the potential to undergo both symmetric and asymmetric cell divisions, and appropriately alter their division patterns in response to environmental cues (Morrison & Kimble 2006).

Asymmetric cell divisions produce two daughter cells of different 'types'. For stem cells this typically means the production of one self-renewing daughter cell (i.e. another stem cell) and one differentiated daughter cell that does not retain self-renewal potential. By contrast, symmetric stem cell divisions produce two daughter cells of the same type: either two stem cells, or two progenitor cells that have undergone the first step of commitment. Because asymmetric cell divisions produce one stem cell per division, they are a natural way to maintain stem cell numbers while simultaneously producing differentiated progeny, and have accordingly been widely studied as a mechanism for maintaining tissue homeostasis (Yamashita et al. 2010). However, there is growing evidence that tissue homeostasis can also be maintained by balancing different kinds of symmetric divisions within the stem cell pool (Simons & Clevers 2011). In particular, if the propensity for each stem cell to divide symmetrically to produce two committed progenitors is equal to the propensity to symmetrically divide to produce two stem cells then the expected number of stem cells will not change. In this case, the propensities for different kinds of symmetric and asymmetric divisions must be tightly controlled to ensure an appropriate stem cell pool is maintained with age. Failure of this control can have dramatic consequences for the organism. For example, various different types of cancer, including leukemia, can be caused by loss of balance in cell division patterns (Alcolea et al. 2014, Frede et al. 2016, Stiehl & Marciniak-Czochra 2017, Wu et al. 2007, Zimdahl et al. 2014).

To achieve this control, HSC dynamics are regulated by extracellular signals from the specialized bone marrow microenvironment(s), or niche(s), in which they reside (Moore & Lemischka 2006, Wilson & Trumpp 2006). Instruction from the niche appears to be particularly important for maintaining tissue homeostasis by producing a stem cell population that is quiescent under normal circumstances, yet poised to initiate appropriate rapid tissue expansion when needed – for example, on exposure to stress stimuli (Trumpp et al. 2010, Mendelson & Frenette 2014, Prendergast & Essers 2014, Karigane et al. 2016, van Galen et al. 2014).

Importantly, the ability of individual HSCs to respond appropriately to niche stimuli declines with age and aging is, accordingly, accompanied by a loss of balance of mature cell types and the accumulation of phenotypically defined HSCs (Morrison et al. 1996, Sudo et al. 2000, Rossi et al. 2005, Dykstra et al. 2011, Pang et al. 2011). Both cell-intrinsic and cell-extrinsic mechanisms are thought to contribute to this loss of balance (Mejia-Ramirez & Florian 2020, Ho & Méndez-Ferrer 2020). For example, when HSCs from aged mice are transplanted into young mice they maintain aged characteristics, including decreased lymphopoiesis (Morrison et al. 1996, Rossi et al. 2005, Dykstra et al. 2011), suggesting cell-intrinsic aging mechanisms. These intrinsic mechanisms may relate to the accumulation of mitochondrial and/or genomic DNA damage which naturally occurs with age, even in quiescent HSCs (Norddahl et al. 2011, Beerman et al. 2014). Indeed, there is evidence that such damage leads to increased propensity for symmetric cell divisions and proliferative exhaustion of the stem cell pool (Insinga et al. 2013). Similarly, broad epigenetic changes may also accumulate which entrench aged HSCs in a disturbed divisional state (Sun et al. 2014), marked by reduced cell polarity and symmetric inheritance of epigenetic marks (Florian et al. 2018).

In contrast, transplantation of young HSCs into old mice yields low re-population efficiency, indicating that age-related changes to the stem cell microenvironment also occur and these changes affect the ability to HSCs home and maintain their activity (Rossi et al. 2005, Guidi et al. 2017, Ho & Méndez-Ferrer 2020). For example, recent findings indicate that extrinsic signals from osteoblasts, such as Angpt1, Kitl, Opn and Jag2 are important for regulating HSC dynamics (Arai et al. 2004,

Zhang et al. 2019, Guidi et al. 2017, Saçma et al. 2019) and that aging alters this signalling (Guidi et al. 2017). Ectopic expression of factors characteristic of young niche cells have accordingly been seen to rejuvenate the bone marrow and improve HSC engraftment (Guidi et al. 2017, Nakahara et al. 2019).

Collectively, these results indicate that HSC dynamics are regulated by a complex interplay between cell-intrinsic and cell-extrinsic mechanisms that alter substantially with age. However, the nature of this interplay is not completely understood. Here, we sought to address this issue using single cell profiling, machine-learning and *in vivo* functional studies to dissect divisions of individual HSCs and explore how division patterns change with age and in response to niche instruction.

RESULTS

To approach this issue we used a reporter mouse, in which long-term repopulating HSCs (LT-HSCs) are marked by GFP expression driven by the ectopic viral integration site 1 (Evi1) promoter (Kataoka et al. 2011). We have validated this mouse model comprehensively (see **Supplemental Figures S1 and S2**). To summarise briefly, we confirmed that the LSKCD41^{-}CD48^{-}CD150^{+}CD34^{-} Evi1-GFP^{+} bone marrow fraction (denoted Evi1^{+}) consist of a homogenous population of LT-HSCs (**Supplemental Figure S1A-S1G**), with high repopulation activity (**Supplemental Figure S1H-S1I**), and therefore presents a suitable model to investigate the influence of the stem cell niche on HSC self-renewal and aging.

To investigate the dynamics of individual HSCs we conducted an *ex vivo* paired daughter cell (PDC) assay, that uses single cell gene expression profiling to compare differences in expression patterns between daughter cells arising from divisions of Evi1^{+} LT-HSCs. A schematic of our PDC assay is given in **Supplemental Figure S2A**. Briefly, individual Evi1^{+} LT-HSCs were seeded on to fibronectin (FN)-coated plates and cultured in serum-free medium with Stem Cell Factor (SCF) and Thrombopoietin (TPO), with or without the niche factor Angiopoietin-1 (Angpt1) for two days to allow them to divide. We focused our attention on the role of Angpt1 since it has previously been shown to enhance HSC quiescence and self-renewal (Arai et al. 2004). While SCF and TPO may also have important roles in regulating HSC division asymmetry, we did not investigate them explicitly. More than 90% of HSCs were observed to divide only once within two days. We did not observe any evidence of distinct sub-populations of cells that were either highly proliferative or slow-dividing, although our selection strategy does not exclude this possibility. After two days of culture, wells that contained precisely two cells were identified, daughter cells were separated using a micro-manipulator, and immediately profiled for expression of a panel of 96 HSC-self-renewal and lineage commitment associated genes using qPCR arrays (96·96 Dynamic Array, BioMark^{TM} system, Fluidigm, see **Supplemental Table S1** for a detailed list of genes and primers used). Because gene expression patterns for both daughter cells from each single HSC division were obtained, we were able to compare their patterns of gene expression, and explore how multivariate associations between daughter cells were affected by culture conditions. It is important to note that this assay focuses on division-dependent HSC differentiation, but does not assess direct, cell division-independent, differentiation which may also be important (Grinenko et al. 2018).

Analysis of expression patterns in paired daughter cells indicated that Angpt1 has a widespread, combinatorial affect on both gene expression and expression asymmetry patterns (**Supplemental Figure 2**). However, the effect of Angpt1 on expression asymmetry was difficult to detect using conventional statistical methods (**Supplemental Figure S2**). Therefore, we sought to investigate the effect of Angpt1 on division patterns using a supervised machine learning approach.

Machine learning of cell identities from single cell expression data

We first constructed a training library of single cell expression patterns from which we were able to benchmark the expected cell-cell variability in expression patterns that arises when profiling various different defined cell populations. Specifically, we isolated a range of different types of hematopoietic stem and progenitor cells from young (4-week-old), adult (8-week-old) and aged (18-month-old) mice. In total we selected nine different stem and progenitor populations. Details of our selection procedures are given in **Figure 1A** and the **STAR Methods**. Details of the abbreviations used to identify these populations are

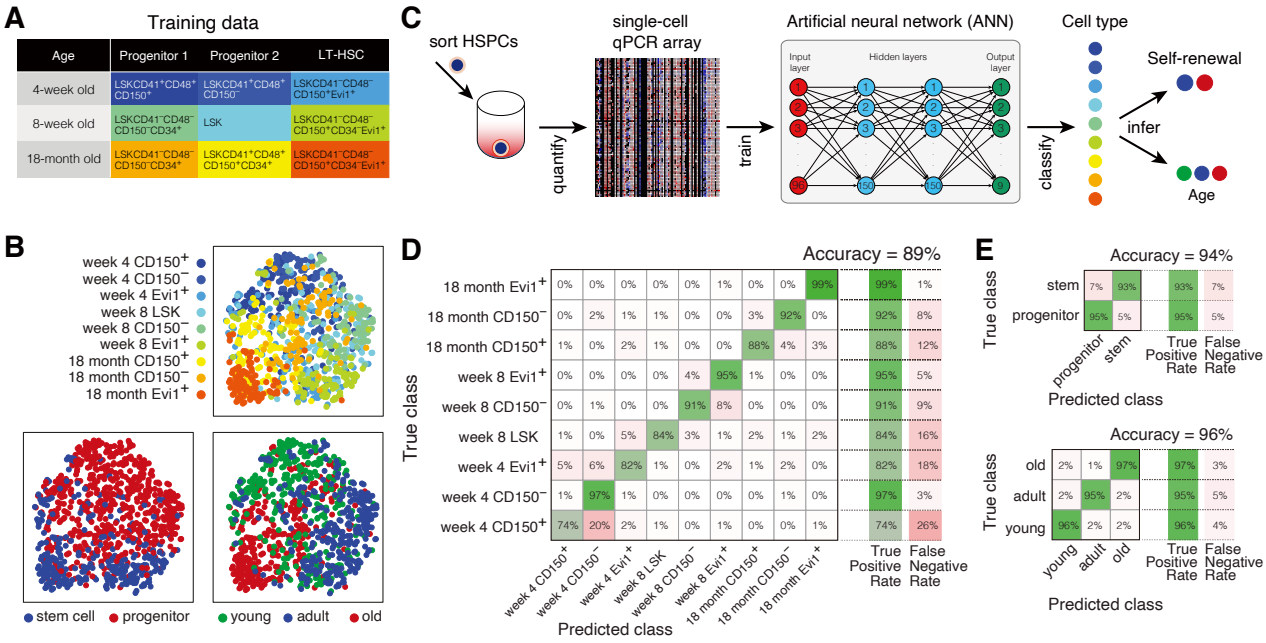

Figure 1. Machine learning of cell identities from single cell expression data. (A) Selection protocols for training data. For each training class 96 cells were selected from pooled samples isolated from 3 mice.

(B) Dimensionality reduction of training data using t-SNE (Van Der Maaten et al. 2009). Training data sets exhibit broad patterns of gene expression and are not easily distinguished from one-another with unsupervised methods. (C) Schematic of machine learning protocol. An artificial neural network (ANN) was trained to distinguish between cells from training samples based on their patterns of gene expression. Once trained the ANN was able to predict the identity, and hence also self-renewal ability and 'age', of individual cells. (D-E) The trained ANN is able to reliably identify cells from their expression patterns. (D) Confusion matrix for the ANN classifier, indicating high (89%) overall accuracy. (E) When restricted to regenerative status (confusion matrix, top) or age (confusion matrix, bottom) classification accuracy further improves.

given in the **STAR Methods**. Immediately after isolation we profiled individual cells in these populations for the same panel genes that we used in the PDC experiments using the same single cell qPCR assay. Thus, we obtained samples of single cell expression patterns for a range of cell types in the hematopoietic hierarchy, taken from mice at different stages of development. These sample data sets provided us with a training library from which we were able to learn the natural variation in gene expression present in each of these populations, and how gene expression patterns compare across the populations and ages. All single cell data was normalized prior to analysis (see **STAR Methods**).

Unsupervised analysis of this training data indicated that each population was highly variable in its expression patterns (**Figure 1B**). While distinct trends were apparent – for example cells taken from mice of the same age tended to be similar to each other, see **Figure 1B, middle panel**; as were stem cells from mice of all ages, see **Figure 1B, right panel** – these associations were diffuse and highly combinatorial, making it difficult to discriminate between the populations using traditional statistical methods.

To progress further, we trained an artificial neural network (ANN) to accurately discriminate between the different training cell types based on their patterns of expression. ANNs are highly effective at pattern recognition and can substantially out-perform classical statistical procedures when properly trained (Friedman et al. 2001, Goodfellow et al. 2016). Details of the architecture and training of our ANN are given in the **STAR Methods** and summarized schematically in **Figure 1C**. Cross-validation was used to avoid over-fitting and ensure that the classifier identified biological, rather than technical, features.

We found that our ANN was able to recognize all the different kinds of stem and progenitor cells profiled, and simultaneously predict the age of the mouse from which they were isolated, with 89% overall accuracy. The confusion matrix for cross-validated predictions is given in **Figure 1D**. When restricted to predicting the regenerative status of the cell (i.e. is it a stem or progenitor cell?) or predicting the age of the cell (i.e. was it taken from a young, adult or aged mouse?), accuracy increased to 96% and 94% respectively. Confusion matrices for cross-validated predictions of regenerative status and age are given in **Figure 1E**.

These results show that although gene expression patterns are highly variable, and variations in expression patterns between different types of stem and progenitor cells are highly combinatorial, machine learning methods can be used to benchmark this variability and accurately predict individual cell identities directly from their gene expression profiles.

Angpt1 maintains HSC self-renewal *in vitro*

To investigate the nature of HSC divisions we used our trained ANN to determine the identities of the daughter cells produced from our PDC experiments. Because our ANN assigns each daughter cell to one of nine different categories, we were able to classify each division into one of 81 (9×9) different categories, representing a range of different kinds of symmetric and asymmetric divisions, as well as predict the developmental state each daughter cell to determine if they had acquired aging-associated characteristics through division (**Figure 2A**). It is important to note that these predictions relate to the identity of the daughter cell immediately after division in culture, which may be transient or be perturbed upon subsequent environmental stimulus.

By analyzing PDC division patterns we found that LT-HSCs taken from 8-week-old mice typically divided to produce a range of daughter cells with different regenerative potentials and predicted 'ages' (**Figure 2B**). In both control and Angpt1 treated conditions the most common divisions produced were ones in which: (1) both daughter cells identified as belonging to the Evi1$^+$ population from 8-week-old mice. These divisions represent symmetric stem-stem (S-S) divisions in which both daughter cells retain the same regenerative status and age-associated characteristics of the parent LT-HSC; (2) one daughter cell is classified as an 8-week-old Evi1$^+$ LT-HSC, and one daughter is classified as an 18-month-old LSKCD41$^+$CD48$^+$CD34$^+$CD150$^+$ progenitor cell. These divisions represent asymmetric stem-progenitor (S-P) divisions in which one daughter cell retains the same regenerative status and age characteristics of the parent LT-HSC and one daughter acquires a partially differentiated status and characteristics associated with aging; (3) both daughter cells are classified as 18-month-old LSKCD41$^+$CD48$^+$CD34$^+$CD150$^+$ progenitor cells. These divisions represent symmetric progenitor-progenitor (P-P) divisions in which both daughters differentiate

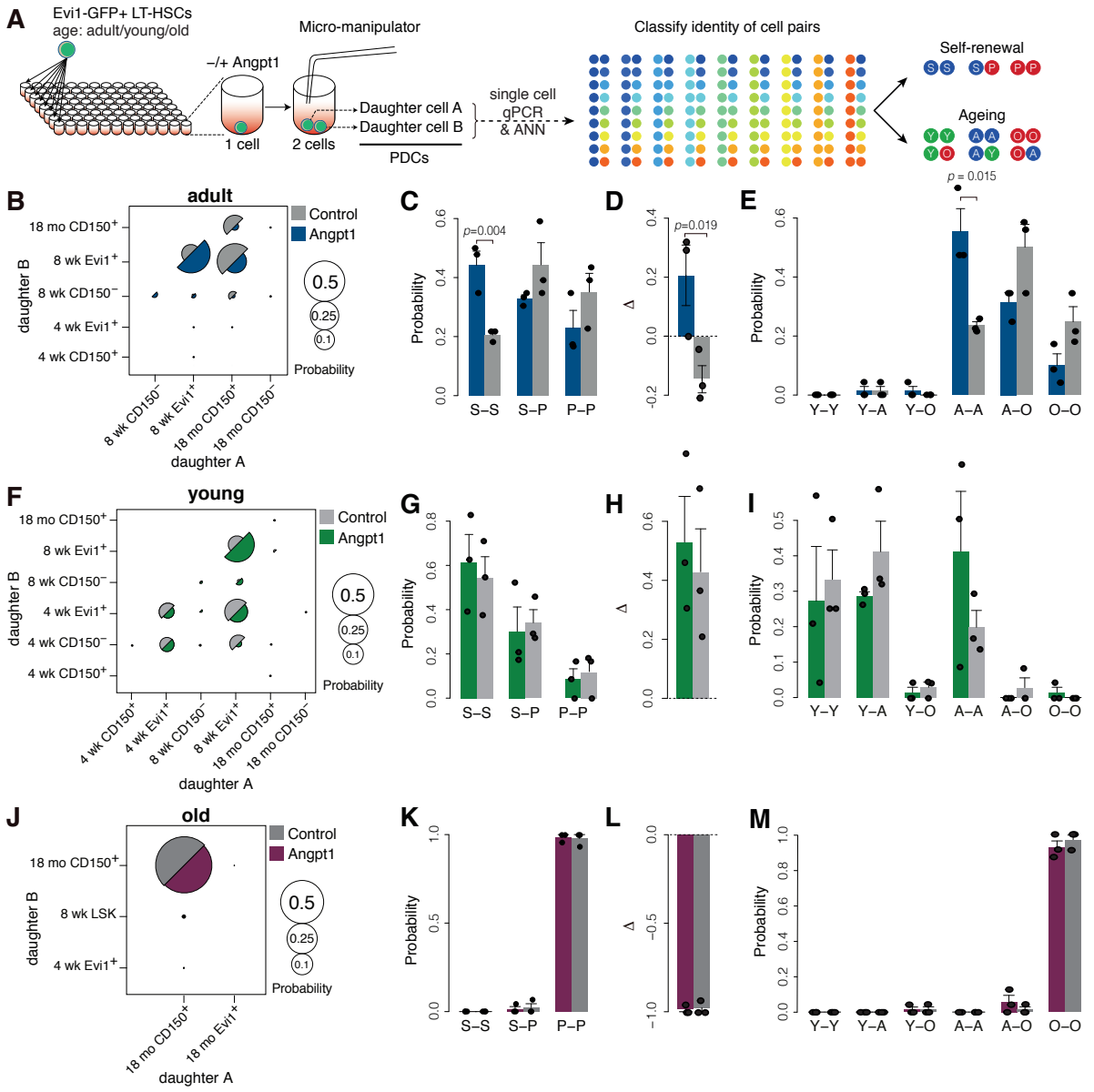

Figure 2. Machine learning of stem cell divisions. (A) Classification of paired daughter cell (PDC) divisions using the trained ANN. Outcome of divisions from adult (B-E; 8-week-old mice), young (F-I; 4-week-old mice), and old (J-M; 18-month-old mice) stem cells. (B,F,J) Division probabilities. Daughter cell identities are not ordered. Note that axes are not equivalent: labels are chosen to show all outcomes observed while avoiding white space. The smallest markers represent one cell. (C,G,K) Classification of PDC divisions using the trained ANN, restricted to regenerative status. (D,H,L) The expansion factor Δ. When $\Delta > 0$ the stem cell pool is expanding; when $\Delta < 0$ the stem cell pool is depleting. (D) Δ becomes positive upon Angpt1 treatment in stem cells from adult mice, indicating that these cells are sensitive to niche instruction. (H) $\Delta > 0$ in both control and Angpt1 treated cells indicating robust expansion of the stem cell pool in young mice. (L) $\Delta < 0$ in both control and Angpt1 treated cells indicating rapid depletion of the stem cell pool in old mice. (E, I, M) Classification of PDC divisions using the trained ANN, restricted to age. (E-I) Spontaneous acquisition of aging-associated characteristics is commonly observed in one or other, or both, daughter cells. Spontaneous rejuvenation is never observed, to within the accuracy of the classifier. In adult LT-HSCs, Angpt1 treatment inhibits cellular aging *in vitro*. (M) Daughter cells of old stem cells have age-associated characteristics in both control and Angpt1 treated conditions. In panels B-M, 144-288 pairs of cells were analyzed for each age from pooled LT-HSC samples obtained from 3-4 experiments, each using 2-3 mice.

and both acquire characteristics associated with aging.

However, while similar kinds of division were seen in both culture conditions, the balance of probabilities was significantly altered upon Angpt1 treatment (**Figures 2C-2E**). Considering the regenerative status of the daughter cells (without regard for their predicted age-associated characteristics) we found that the total proportion of cells undergoing asymmetric S-P self-renewal divisions was not significantly affected by Angpt1 treatment. This is in accordance with our previous unsupervised analysis of gene expression patterns, which found that Angpt1 did not substantially affect the symmetry of divisions (**Supplemental Figure S2**). However, our ANN analysis revealed that the proportion of symmetric S-S divisions was significantly increased by Angpt1 treatment (**Figure 2C**), a feature that was not apparent using unsupervised methods. These results suggest that Angpt1 treatment might affect stem cell numbers by stimulating symmetric S-S divisions.

This is notable because a simple mathematical analysis of cell proliferation dynamics (see **Supplemental Material: Mathematical Modeling**) indicates that maintenance of the stem cell pool is critically determined by the relative propensity of symmetric S-S and P-P divisions. In particular, if the probability p_1 of an S-S division is greater than the probability p_2 of a P-P division then the stem cell pool will expand. Similarly, if p_2 is greater than p_1 then the pool will deplete. Thus, the rate of expansion or depletion of the stem cell pool is determined by the difference $\Delta = p_1 - p_2$. We found that the expansion parameter $\Delta < 0$ in control conditions, yet $\Delta > 0$ upon Angpt1 treatment (**Figure 2D**), indicating that Angpt1 treatment may sustain stem cell self-renewal *ex vivo* by specifically stimulating symmetric S-S divisions.

We also used our ANN to determine composition of the Evi1$^-$ population. Consistent with statistical analysis of the relative variability of the Evi1$^+$ and Evi1$^-$ populations (**Supplemental Figure S1F-G**), our ANN classifier predicted that the Evi1$^-$ fraction contains a mixture of stem and progenitor cell populations (**Supplemental Figures S3B-C**).

Ex vivo culture induces spontaneous acquisition of aging-associated characteristics from the first cell division

In addition to predicting regenerative status our ANN was also able to predict the developmental state of cell. To investigate how culture affects aging-associated characteristics we therefore also used our ANN to investigate the predicted developmental state of PDCs. Depending on its similarity to cells in the training library we classified each daughter cell as being 'young' (most similar to a cell taken from a 4-week-old mouse, denoted Y), 'adult' (most similar to a cell taken from an 8-week-old mouse, denoted A) or 'old' (most similar to a cell taken from an 18-month-old mouse, denoted O), and thus classified each LT-HSC division into one of nine possible classes depending on the identities of the two daughter cells: young-young (Y-Y), young-adult (Y-A), young-old (Y-O), adult-adult (A-A), adult-old (A-O), or old-old (O-O). We emphasise that this categorization does not imply equality: so, for example, cells that are categorized as 'old' have not necessarily acquired fully aged characteristics, but rather are more similar to cells from 18-month-old mice than those from 4- or 8-week-old mice.

We first noted that while it is theoretically possible for daughter cells from divisions of LT-HSCs taken from 8-week-old adult old mice to acquire a younger developmental state in culture, such spontaneous rejuvenation did not occur in practice (**Figure 2E**). However, while both daughters were commonly identified as being adult cells, we also observed that spontaneous aging of one or other (or both) daughter cells also occurred with significant regularity (**Figure 2E**). This indicates that cell culture induces accelerated cellular aging in the progeny of LT-HSCs from the very first division. Indeed, in control conditions approximately 50% of cells showed spontaneous aging through the first division (**Supplemental Figure S3E**). However, we also observed that this spontaneous aging was significantly inhibited upon Angpt1 treatment (**Figures 2E, S3E**), suggesting that it is a feature of culture that is not inevitable, but can be controlled.

HSC self-renewal ability and sensitivity to niche instruction is rapidly lost in culture

To determine how effective Angpt1 was at controlling aging in culture we examined associations between paired granddaughter cells (PGDCs; **Supplemental Figure S4A**). Cells were cultured exactly as for the PDC assay. Wells that contained precisely

two cells after two days in culture were identified and daughter cells from these first divisions were separated with a micromanipulator, re-plated cultured for two more days and allowed to divide a second time in the same culture conditions. As before, wells that contained precisely two cells were identified, and granddaughters were separated and profiled for expression of the same panel of 96 genes.

Consistent with the results of the PDC assay, we observed that almost all secondary divisions produced granddaughter cells that had lost stem cell status (**Supplemental Figure S4B**), and more than 70% of secondary divisions produced at least one granddaughter cell with age-associated characteristics in both control and Angpt1 treated cultures (**Supplemental Figure S4C**). In contrast to the PDC results, we found that Angpt1 did not significantly alter secondary division patterns with respect to regenerative status (**Supplemental Figure S4B**). However, in accordance with PDC results, Angpt1 treatment was associated with a modest reduction of acquisition of age-associated characteristics (**Supplemental Figure S4C**). Furthermore, because the propensity for P-P divisions dominated the propensity for S-S divisions in secondary divisions, we found that the expansion parameter $\Delta = p_1 - p_2$ was negative for secondary divisions in both control and Angpt1 treated conditions, indicating that neither condition is able to support sustained stem cell self-renewal beyond one division.

Collectively, these results suggest that freshly isolated HSCs retain an intrinsic sensitivity to external stimuli which allows them to respond to supplementation of niche factors *in vitro*. However, they rapidly lose this sensitivity, and simultaneously gain age-associated characteristics, when cultured *ex vivo*.

Stem cell self-renewal potential declines with age

We next sought to dissect how division patterns and niche sensitivity evolve with age. To do so, we conducted further PDC experiments using LT-HSCs taken from young (4-week-old) and aged (18-month-old) mice and again used our ANN to investigate daughter cell characteristics. Clustering analysis of the combined training and PDC data are provided in **Supplemental Figure S5**.

When we examined division pattern of LT-HSCs taken from 4-week-old mice, we found that they differed substantially from those of HSCs taken from 8-week-old mice (compare **Figures 2B, 2F**). In both control and Angpt1 treated conditions the most common divisions of 4-week-old HSCs were those that produced: (1) two daughter cells both identified as belonging to the Evi1$^+$ population from 4-week-old mice (**Figure 2F**). These divisions represent symmetric S-S divisions in which both daughter cells retain the same regenerative status and age characteristics of the parent LT-HSC; (2) one daughter cell is identified as belonging to the Evi1$^+$ population from 4-week-old mice and the other is identified as belonging to the Evi1$^+$ population from 8-week-old mice. These divisions represent symmetric S-S divisions in which one daughter cell acquires characteristics associated with aging.

Considering only the regenerative status of the daughter cells we found that symmetric S-S divisions predominated over S-P and P-P divisions (**Figure 2G**), resulting in a positive expansion parameter Δ (**Figure 2H**), in both control and Angpt1 treated conditions, indicating that young HSCs have an inherent ability to expand their numbers independent of the culture conditions. Perhaps because of this inherent bias toward S-S divisions, Angpt1 did not significantly affect division patterns (**Figure 2G**) or significantly affect expansion dynamics (**Figure 2H**).

As with adult LT-HSCs we observed that young LT-HSCs underwent spontaneous aging from the first division in culture, with approximately 50% of divisions giving rise to a cell with adult (i.e. 8-week-old) characteristics (**Figures 2F, 2I, S3D**). However, daughter cells did not readily take on characteristics of old (i.e. 18-month-old) cells, suggesting that aging is a gradual process that advances through multiple cell divisions. While we did observe an apparent increase in acquisition of aging-associated characteristics upon Angpt1 treatment (see **Figures 2F, 2I, S3D**), these differences were not statistically significant. Thus, in accordance with its effect on regenerative status, Angpt1 treatment did not appear to have a strong effect on the age character of cells from young mice (**Figures 2I, S3D**).

In contrast to LT-HSCs taken from 4- and 8-week-old mice, LT-HSCs taken from 18-month-old mice divided almost

exclusively to produce two cells with progenitor characteristics (**Figures 2J-2L**), resulting in a negative expansion parameter Δ (**Figure 2L**), suggesting that although these aged cells have the immunophenotypic characteristics of stem cells, they have lost the ability to self-renew *in vitro*. Furthermore, old LT-HSCs almost exclusively produced old daughter cells (**Figure 2M**), and we did not see spontaneous rejuvenation to a younger phenotype, to within the error of the classifier. Very similar division patterns were observed in control and Angpt1 treated cultures, suggesting that, like young LT-HSCs, aged LT-HSCs are insensitive to niche instruction via Angpt1 *in vitro* (**Figures 2I-2M**).

It is notable that our ANN assigns exactly one cell identity to each daughter cell based upon the posterior probabilities produced by the softmax function in its output layer. The mean posterior probabilities for the assigned identities for the young, adult and old daughter cells were: 0.76, 0.79 and 0.97 respectively, indicating that our classifier is able to reliably predict cell identities. Future analysis that takes into account the spread of probabilities over the different possible identities may provide further insight to the diversity of cellular identities present in the HSC pool, but was not pursued further here.

In addition to using our ANN to investigate PDC patterns, we also used it to determine composition of the Evi1-GFP^{-} population from young and aged mice. We observed that the proportion of Evi1-GFP^{-} cells classified as Evi1^{+} increases with age, indicating that these two populations are initially quite distinct but become more alike in their gene expression patterns over time (**Supplemental Figure S3B-C**). Consistent with these results we found that while Evi1 apparently still enriches for functional HSCs in old mice, the regenerative potency of these HSCs is substantially diminished with respect to HSCs taken from 8-week-old mice (**Supplemental Figure S6**).

Collectively, these results indicate that LT-HSC division patterns vary considerably with age, with regenerative potency being gradually lost, and response to Angpt1 being maximized through the middle of life. We found that the Angpt1 receptor Tie2 was consistently expressed in hematopoietic stem and progenitor cells throughout development and aging (**Supplemental Figure S7A-B**) and the percentage of Evi1^{+} cells within the LSKCD41^{-}CD48^{-}CD150^{+}CD34^{-} fraction increases with age (**Supplemental Figure S7C**). In support of our PDC analysis, these results indicate that the observed changes in division patterns are not directly due to changes in sensitivity to niche instruction or loss of stem cell numbers *per se* but rather are due to an evolving balance between cell-intrinsic and extrinsic regulatory mechanisms.

Substrate stiffness regulates LT-HSC division patterns

To investigate HSC division dynamics further we also sought to determine how the physical structure of the niche affects HSC behaviour. To do so we manufactured a bespoke polyethylene glycol (PEG) microwell culture system, which provides a softer environment with a high water content that more closely matches the physical characteristics of the *in vivo* HSC niche than standard culture conditions (Gobaa et al. 2011, Lutolf et al. 2009, Roch et al. 2017). Similar niche constructs have been shown to support stem cell self-renewal in other contexts (Gilbert et al. 2010).

To test the effect of our artificial niche on division patterns we conducted our PDC assay using 8-week-old Evi1^{+} LT-HSCs seeded onto our FN-coated PEG hydrogel micro-wells with or without Angpt1. In the absence of Angpt1 we found that this culture system stimulated symmetric S-S divisions, resulting in a net expansion of the HSC pool (**Supplemental Figures S8A-S8C**), indicating that it is more supportive of HSC self-renewal than standard culture conditions. Angpt1 treatment did not significantly alter division patterns, perhaps because symmetric S-S divisions were already enhanced by the PEG micro-well niche. In accordance with our results from standard culture conditions we observed spontaneous aging, albeit at a lower rate, with approximately 20-30% of cells adopting age-associated characteristics after one division in micro-well culture (**Supplemental Figures S8D-S8E**). However, in contrast to standard culture conditions, we also observed spontaneous rejuvenation of a small proportion of cells in both control and Angpt1 treated cultures, and saw that Angpt1 treatment appeared to weakly inhibit the aging process, significantly reducing the proportion of divisions that gave rise to two daughter cells with age-associated characteristics (**Supplemental Figure S8D**).

These results indicate that freshly isolated LT-HSCs are sensitive to both physical and biochemical stimulation by the niche,

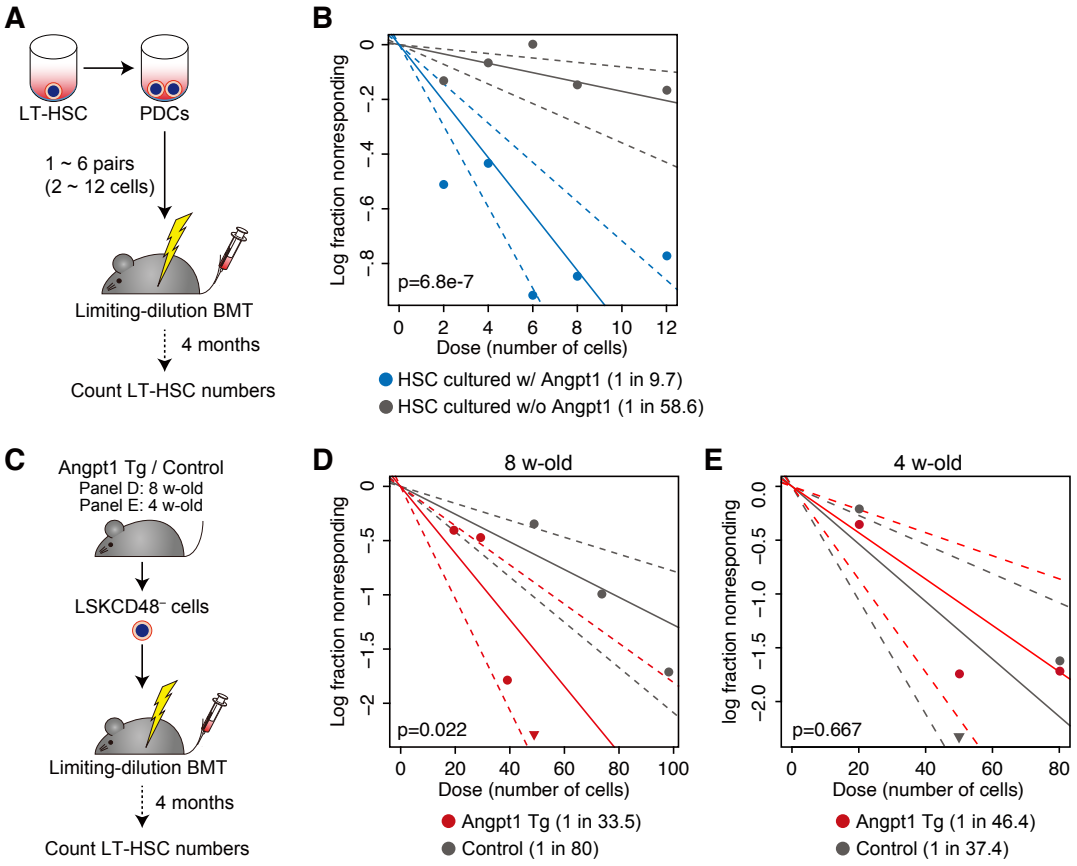

Figure 3. Angpt1 enhances functional stem cell activity *ex vivo* and *in vivo*. (A) Schematic of limiting dilution bone marrow transplantation (BMT) assay. (B) Limiting dilution BMT of cultured PDCs shows that Angpt1 treatment maintains HSC activity *ex vivo*. The following number of mice (n) were used: $n = 8$, control 1 pair (2 cells); $n = 15$, control 2 pairs (4 cells); $n = 5$: control 3 pairs (6 cells); $n = 22$, control 4 pairs (8 cells); $n = 13$, control 6 pairs (12 cells); $n = 10$, Angpt1 1 pair (2 cells); $n = 17$, Angpt1 2 pairs (4 cells); $n = 5$, Angpt1 3 pairs (6 cells); $n = 21$, Angpt1 4 pairs (8 cells); $n = 13$, Angpt1 6 pairs (12 cells). (C) Schematic of limiting dilution BMT assay in osteoblast-specific Angpt1 transgenic (Tg) mice. (D-E) Limiting dilution BMT in osteoblast-specific Angpt1 Tg mice shows that Angpt1 enhances HSC activity *in vivo* in adult (8-week-old) mice (panel D) but not during development (panel E). The following number of mice (n) were used in panel D: $n = 10$, control 50 cells; $n = 8$, control 75 cells; $n = 11$, control 100 cells; $n = 6$, Angpt1 Tg 20 cells; $n = 8$, Angpt1 Tg 30 cells; $n = 6$, Angpt1 Tg 40 cells; $n = 5$, Angpt1 Tg 50 cells. The following number of mice (n) were used in panel E: $n = 5$, control 20 cells; $n = 5$, control 50 cells; $n = 5$, control 80 cells; $n = 5$, Angpt1 Tg 20 cells; $n = 5$, Angpt1 Tg 50 cells; $n = 5$, Angpt1 Tg 80 cells. p-values are from extreme value limiting dilution analysis (ELDA) (Hu & Smyth 2009) in all panels. Dotted lines give 95% confidence intervals and triangles show data points with zero mice nonresponding.

and variation of the physical characteristics of the culture environment may overcome the culture-induced loss of sensitivity to niche instruction and premature aging that we observed in standard culture conditions.

Angpt1 increases long term reconstitution in vivo

Taken together our results suggest that Angpt1 treatment *in vitro* partially protects LT-HSCs from cellular aging, and increases the propensity for symmetric S-S divisions that expand the HSC pool. To investigate this further we sought to assess the

regenerative capacity of paired daughter cells *in vivo*. We performed limiting dilution bone marrow transplantation (BMT) of PDCs. As before, individual Evi1$^+$ LT-HSCs were isolated from 8-week-old mice and seeded onto FN-coated plates and cultured in serum-free medium with SCF and TPO, with or without Angpt1 for two days. After two days of culture, daughter cells were pooled and 1, 2, 3, 4, or 6 pairs of PDCs from the pool were transplanted into lethally irradiated mice. The proportion of LT-HSCs in the transplanted daughter cells was estimated from the fraction of non-responding mice (**Figure 3A**). Consistent with the results of our ANN classifier, we observed that culture with Angpt1 increased the proportion of LT-HSCs nearly 6-fold, from 1 in 58.6 transplanted cells without Angpt1 treatment to 1 in 9.7 with (**Figure 3B**). A similar analysis using PDCs cultured in our bespoke PEG micro-well also confirmed the enhanced ability of this culture system to maintain stem cell numbers *ex vivo* (**Supplemental Figure S9**; an alternative presentation of both these data is provided in **Supplemental Figure S10**).

In addition to determining the effect of Angpt1 on cultured cells we also evaluated its role in regulating LT-HSC numbers *in vivo*. To do so, we isolated LSKCD48$^-$ cells from 8-week-old osteoblast-specific Angpt1 transgenic (Tg) (Col1a1-Cre(+) ; CAGp-IND-COMP-Angpt1) and control (Col1a1-Cre(–) ; CAGp-IND-COMP-Angpt1) mice and assessed the regenerative function of these cells via limiting dilution BMT (**Figure 3C-D**). By analyzing the fraction of non-responding mice subsequent to BMT we were able to estimate the proportion of LT-HSCs in the LSKCD48$^-$ fraction. We found that LT-HSC incidence was significantly higher in adult Angpt1 Tg mice than controls (1 in 33.5 cells for Tg mice, compared to 1 in 80 for controls, see **Figure 3D**). However, when we conducted similar limiting dilution BMT on LSKCD48$^-$ cells from juvenile (4-week-old) osteoblast-specific Angpt1 Tg mice we did not observe any difference in LT-HSC numbers (**Figure 3E**), indicating that Angpt1 regulation of stem cell numbers is age-dependent.

Immunohistochemical staining of VE-cadherin$^+$ blood vessels in the BM indicated that total vessel length was comparable in Angpt1 Tg and control mice (**Supplemental Figure S11**), suggesting that Angpt1 does not boost stem cell numbers in adult Angpt1 Tg mice by enlarging the HSC niche. Rather, these results are in agreement with our PDC analysis, and indicate that Angpt1 maintains stem cell activity *in vivo* by stimulating symmetric S-S divisions in the stem cell pool.

Model sensitivity analysis

To investigate this balance further we sought to identify gene expression patterns that were particularly associated with each cell identity and determine how these patterns changed with age. In a traditional statistical setting such analysis would involve identifying genes that are either up- or down-regulated in each different cell type. From a machine-learning perspective the process of characterising different cell types based upon combinations of up- and down-regulated genes is an example of a decision-tree classifier (Friedman et al. 2001). However, decision-trees are typically not able to solve complex classification problems (although methods based on ensembles of decision trees often are (Friedman et al. 2001)) and indeed we found that this process did not allow us accurately dissect HSC division patterns (see **Supplemental Figure S1**). To overcome this problem we used an ANN to assign cellular identities based upon combinatorial patterns of gene expression. However, due to the highly nonlinear nature of the ANN decision-making process it is not naturally associated with subsets of up- and down-regulated genes. To interpret the decision-making process of our ANN we therefore sought to conduct a sensitivity analysis to identify features of importance. To do so we used LIME (Local Interpretable Model-agnostic Explanations) to systematically dissect the genes that were most important when making the decision to assign individual PDCs to each class (stem/progenitor cell type) (Ribeiro et al. 2016). Although our ANN is highly nonlinear, and involves all the genes profiled, LIME approximates its output locally around each PDC prediction with an interpretable sparse model involving only those genes that were most important for classifying that particular cell. **Figure 4** summarizes this analysis and shows the sets of genes that were consistently associated with classifying PDCs into each different class. We found that the majority of PDCs were classified into five of the nine possible classes (4-week-old Evi-1$^+$, 4-week-old CD150$^+$, 8-week-old Evi-1$^+$, 8-week-old CD150$^-$ and 18-month-old CD150$^+$) and so we focused our sensitivity analysis on these dominant classes (**Figure 4A**).

This analysis revealed that each cellular identity was associated with distinct patterns of marker genes. For example,

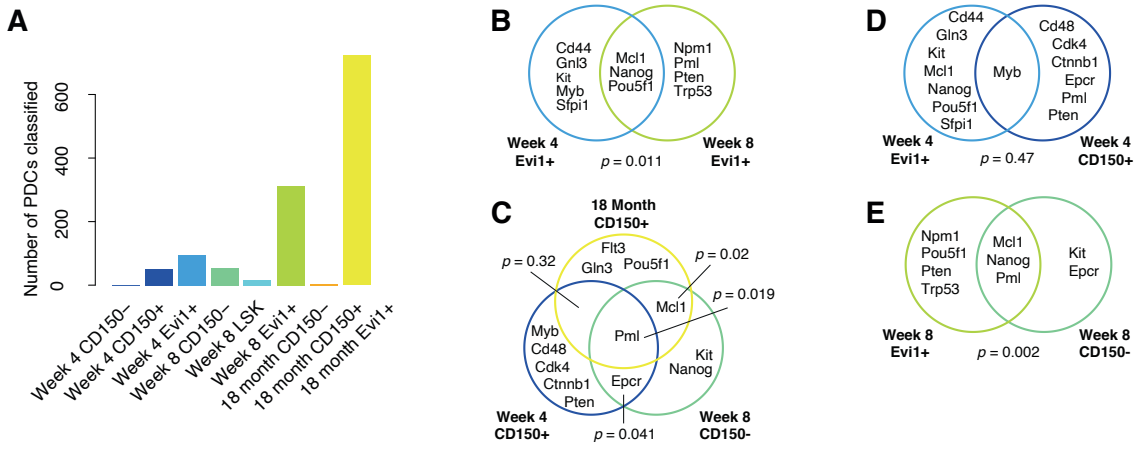

Figure 4. Genes associated with ANN decision-making. (A) The vast majority of PDCs were classified by the ANN into five of the nine possible classes (cell identities). (B-E) Genes identified by LIME to be important in making class-assignments. (B) Intersection of genes associated with the 4-week-old Evi1$^+$ and 8-week-old Evi1$^+$ identities. (C) Intersection of genes associated with the 4-week-old CD150$^+$, 8-week-old CD150$^-$ and 18-month-old CD150$^+$identities. (D) Intersection of genes associated with the 4-week-old Evi1$^+$ and 4-week-old CD150$^+$ identities. (E) Intersection of genes associated with the 8-week-old Evi1$^+$ and 8-week-old CD150$^-$ identities. *p*-values are from permutation tests (1,000 iterations) based upon a sample of 25 cells from each class in all panels.

assignment of PDCs to the young HSC identity was driven by a key set of 8 genes including: *Gln3* which encodes for Nucleostemin, a nucleolar GTP-binding protein that is highly expressed in hematopoietic stem cells (Ali et al. 2017); *Kit*, which encodes for the receptor for SCF and is a positive marker for HSPCs that is involved in maintaining HSC quiescence (Thorén et al. 2008); *Mcl1* which is essential for ensuring the homeostasis of early hematopoietic progenitors (Opferman et al. 2005); and *Myb*, which encodes for c-Myb a transcription factor that is essential for HSC self-renewal (García et al. 2009) and sensitively regulates HSC lineage potential (Sakamoto et al. 2015) (**Figure 4B**). We emphasise that this does not mean that these genes are positively associated with the young HSC identity, but rather that combinatorial differences in the relative expression levels of these genes can be used to distinguish young HSCs from the other cell types.

Similarly the adult HSC identity was also associated with distinct combinatorial patterns of expression of key genes including *Pml*, a tumor-suppressor gene that has a key role in the maintenance of HSCs (Ito et al. 2008) including regulating HSC metabolism (Nakahara et al. 2014), and *Pten*, which plays an essential part in regulating HSC self-renewal, migration, lineage commitment and differentiation (Zhang et al. 2006) (**Figure 4B**). Notably, *Pten* was also significantly asymmetrically partitioned in daughter cells of adult HSC divisions (see **Supplemental Figure S2G**), suggesting that it might have a particularly important role in regulating adult HSC divisions. Putative roles for *Pten* are discussed further in the **Discussion**. The panel of 96 genes that we assessed contains 30 HSC-specific markers, so selection of these markers was not inevitable. Enrichment of identified markers in the subset of HSC-specific genes was significant for both young and adult HSCs ($p = 0.0017$ and $p = 0.0344$ respectively, permutation test).

The sets of genes consistently associated with the adult HSC identity were not disjoint from those associated with the young HSC identity. Three genes – *Mcl1*, *Nanog* and *Pou5f1* – were consistently associated with both identities. This overlap is statistically significant ($p = 0.011$, permutation test), suggesting shared biology. It is notable that both *Nanog* and *Pou5f1* are pluripotent stem cell markers that are well-known to have important roles during development (Chambers et al. 2007, Nichols et al. 1998). While little is known about their function in HSCs, these results suggest that they may also have a role in HSC maturation during development.

Analysis of genes consistently associated with juvenile, adult and aged progenitor cells also identified known regulators including genes encoding for important HSPC cell-surface markers such as *Cd48*, *Procr* and *Flt3* (Kiel et al. 2005, Balazs et al. 2006, Matthews et al. 1991). There was significant overlap of the gene sets associated with progenitor cell identities at different ages, as well as those associated with HSC identities, indicating identification of common regulatory mechanisms (**Figure 4C-E**). Collectively, these results suggest that decisions to assign cell identities by our ANN are not based on technical artefacts but rather upon biologically important, although complex, criteria.

DISCUSSION

There has been longstanding interest in deciphering the mechanisms of stem cell aging and their relationship to aging generally (Geiger et al. 2013, Sharpless & DePinho 2007). It is thought that both cell-intrinsic and cell-extrinsic mechanisms that control the frequency and outcome of cell division events are central to the aging process (Werner et al. 2015, Rossi et al. 2007, Ermolaeva et al. 2018, Ho & Méndez-Ferrer 2020). Here, we have shown that aging alters both the balance in symmetric and asymmetric HSC divisions, and sensitivity of HSCs to niche instruction. Collectively, these changes lead to an expansion of the stem cell pool in early life, balanced niche-responsive self-renewal in adult life, and loss of self-renewal ability in later life.

We found that the niche-factor Angpt1 has a broad effect on the expression of genes associated with PI3K-signalling in HSCs from adult mice – including cell adhesion (*Cdh2*, *Itga2b*), proliferation (*Ccnd1*, *Pbx1*) and metabolism (*Foxo1*) (**Supplemental Figure S2C-D**) – which are known to collectively orchestrate HSC homing and quiescence (Ho & Méndez-Ferrer 2020). In addition, we observed that Angpt1 had subtle combinatorial effects on patterns of gene expression asymmetry (**Supplemental Figure S2F-H**). Expression asymmetry was particularly apparent for *Pten* (**Supplemental Figure S2F-G**), which was also identified in sensitivity analysis of our ANN to be an important regulator of the adult HSC identity. Pten is an antagonist of PI3K (upstream of Akt and mTOR signaling) that is known to cause exhaustion of the HSC pool by stimulating excess cell proliferation when ablated or inactivated through mutation (Yilmaz et al. 2006, Zhang et al. 2006). Thus, asymmetry of partitioning of Pten transcripts may be involved in establishing nascent differences in quiescence and differentiation in daughter cells.

This observation is in accordance with recent work of Loeffler et al. (2019), who used extensive time-lapse imaging of HSC division events to show that lysosomal components are asymmetrically partitioned during mitosis and metabolic differences between daughter cells subsequently emerge. The formation of autophagosomes from lysosomes is important for HSC self-renewal and is tightly regulated by PI3K-signalling (Ito & Suda 2014). Hence, it is possible that Pten has an important part in regulating HSC self-renewal by either reinforcing or dampening the effect of asymmetric segregation of existing lysosomes through control of new autophagosome formation.

While we found that HSCs from both young and adult mice are able to divide both symmetrically and asymmetrically (**Figure 2G** and **Figure 2C**), we observed exclusively symmetric P-P divisions in old mice (**Figure 2K**). This observation is in accordance with previous reports of increased division symmetry in old HSCs, marked by reduced cell polarity and increased activity of Cdc42 (Florian et al. 2012, 2018). Pten may also play a role in modulating Cdc42 activity, via cross-regulation of Wnt signalling (Perry et al. 2011, Sugimura et al. 2012). Based on this collective evidence we anticipate that further investigation Pten as a putative regulatory axis for stem cell aging may prove fruitful.

In addition to alterations in cell-intrinsic mechanisms we also found that the ability of the niche factor Angpt1 to modulate HSC division patterns – and thereby to regulate the number of functional stem cells – varies with age. In particular, sensitivity to niche instruction via Angpt1 is limited to HSCs from adult mice (**Figure 2C-D** and **Figure 3C-E**) and to a lesser extent to young mice (**Figure 2G-H**), while HSCs from old mice remain unresponsive (**Figure 2K-L**). This is in accordance with previous findings of dominant cell intrinsic control of HSC proliferation in old mice (Morrison et al. 1996, Rossi et al. 2005, Dykstra et al. 2011), that is likely related to the concurrent epigenetic changes in the aged HSC genome (Sun et al. 2014).

However, Angpt1 is not the only regulator of HSC proliferation and self-renewal. For instance, we find that physical parameters, such as substrate stiffness, also appear to play a role in regulating the balance of proliferation and differentiation with aging (**Supplemental Figure S9**). These results are in accordance with the known importance of age-related alterations in niche regulation of HSC function (Ho & Méndez-Ferrer 2020, Dorshkind et al. 2019). Collectively our results re-affirm the importance of both cell-intrinsic and extrinsic regulatory mechanisms and indicate that the balance between intrinsic and extrinsic control of HSC proliferation is highly contextual and age-dependent.

Our results also suggest that the proliferative capacity of the stem cells pool as a whole also alters with age. Particularly, symmetric S-S divisions, which expand the stem cell pool, predominate in young HSCs; a balance of symmetric and asymmetric divisions, which maintain homeostasis of the stem cell pool, occur through the middle of life; and symmetric P-P divisions, which deplete the stem cell pool, strongly predominate in later life (**Figure 2D,H,L**).

Because the propensity for symmetric divisions that deplete the stem cell pool increases with age, our results suggest that the stem cell pool will exhaust on aging if it is too proliferative. However, this does not appear to happen. Rather, it has been widely observed that the immunophenotypic stem cell pool increases with age, yet this increase is associated with loss of regenerative potential and increase in linage bias (Pang et al. 2011, Sudo et al. 2000, Rossi et al. 2005, Morrison et al. 1996, Geiger et al. 2013). Thus, our results imply that maintenance of a viable stem cell pool with age requires that stem cells must either: (1) divide rarely, or (2) enter into a state of protective dormancy once their self-renewal ability has been sufficiently compromised.

Both these options are possibilities. It is well-known that the most potent HSCs divide only very rarely *in vivo* – estimates suggest that mouse HSCs divide only once every 145 days or approximately 5 times in a mouse lifetime (Wilson et al. 2008). Similarly, a number of recent reports have found that re-population activity is concentrated in the most quiescent HSC sub-populations (Wilson et al. 2008, Foudi et al. 2009, Takizawa et al. 2011, Qiu et al. 2014) and, furthermore, the accumulation of cell divisions is directly associated with loss of stem cell potency, both during native hematopoiesis and under conditions of stress (Bernitz et al. 2016, Säwén et al. 2016, Qiu et al. 2014, Wilson et al. 2008, Nygren & Bryder 2008, Foudi et al. 2009). Although the precise reasons for this association are unclear, it is likely that HSCs are sensitive to accumulated damage that occurs during repeated cell divisions (Walter et al. 2015). General mechanisms, such as telomere shortening, may also define a 'mitotic clock' that places a fundamental limit on HSC proliferative capacity *in vivo* (Harley et al. 1990, Notaro et al. 1997, Hills et al. 2009, Allsopp, Morin, DePinho, Harley & Weissman 2003, Allsopp, Morin, Horner, DePinho, Harley & Weissman 2003, Werner et al. 2015). There is evidence that such a mitotic clock is encoded reliably enough that individual HSCs are able to 'count' cell divisions enter a dormant state after four divisions (Bernitz et al. 2016).

Such memory mechanisms are consistent with our results, yet we currently know very little about how they work. However, they may be inherent to regulating cellular dynamics with age, and therefore be important in understanding age-related regenerative decline. We anticipate that further investigation of cellular memories – for example using label retention dynamics or genetic labelling strategies in combination with single cell molecular profiling – will be fruitful avenues for future work.

ACKNOWLEDGEMENTS

We would like to thank Dr. Mineo Kurokawa (The University of Tokyo, Japan) for providing Evi1-GFP knockin mice. We also thank Dr. Gou Young Koh (KAIST, Korea) for providing recombinant Angpt1 protein. This research was funded by the funding program for Next Generation World-Leading Researchers (NEXT Program, grant number LS108), Scientific Research (B) (General), grant number 17H04208, from the Ministry of Education, Culture, Sports, Science and Technology (MEXT) of Japan, Takeda Science Foundation, and a donation from Fujino Brain Research, Ltd.

AUTHOR CONTRIBUTIONS

Conceptualization BDM, FA, TS; Methodology BDM, FA; Software BDM, PSS; Formal Analysis BDM, FA, PSS; Investigation, AR, BDM, FA, KH, YMI; Resources MPL; Data Curation BDM, PSS; Writing - Origninal Draft BDM, FA; Writing - Reviewing & Editing BDM, FA, MPL, PSS, TS; Visualization, BDM, PSS; Supervision BDM, FA, MPL, TS; Project Administration, BDM, FA; Funding Acquisition BDM, FA.

DECLARATION OF INTERESTS

The authors declare no competing interests.

References

Alcolea, M. P., Greulich, P., Wabik, A., Frede, J., Simons, B. D. & Jones, P. H. (2014), 'Differentiation imbalance in single oesophageal progenitor cells causes clonal immortalization and field change', *Nature cell biology* **16**(6), 612.

Ali, M. A., Fuse, K., Tadokoro, Y., Hoshii, T., Ueno, M., Kobayashi, M., Nomura, N., Vu, H. T., Peng, H., Hegazy, A. M. et al. (2017), 'Functional dissection of hematopoietic stem cell populations with a stemness-monitoring system based on ns-gfp transgene expression', *Scientific reports* **7**(1), 1–12.

Allsopp, R. C., Morin, G. B., DePinho, R., Harley, C. B. & Weissman, I. L. (2003), 'Telomerase is required to slow telomere shortening and extend replicative lifespan of hscs during serial transplantation', *Blood* **102**(2), 517–520.

Allsopp, R. C., Morin, G. B., Horner, J. W., DePinho, R., Harley, C. B. & Weissman, I. L. (2003), 'Effect of tert over-expression on the long-term transplantation capacity of hematopoietic stem cells', *Nature Medicine* **9**(4), 369.

Arai, F., Hirao, A., Ohmura, M., Sato, H., Matsuoka, S., Takubo, K., Ito, K., Koh, G. Y. & Suda, T. (2004), 'Tie2/angiopoietin-1 signaling regulates hematopoietic stem cell quiescence in the bone marrow niche', *Cell* **118**(2), 149–161.

Balazs, A. B., Fabian, A. J., Esmon, C. T. & Mulligan, R. C. (2006), 'Endothelial protein c receptor (cd201) explicitly identifies hematopoietic stem cells in murine bone marrow', *Blood* **107**(6), 2317–2321.

Beerman, I., Seita, J., Inlay, M. A., Weissman, I. L. & Rossi, D. J. (2014), 'Quiescent hematopoietic stem cells accumulate dna damage during aging that is repaired upon entry into cell cycle', *Cell stem cell* **15**(1), 37–50.

Bernitz, J. M., Kim, H. S., MacArthur, B., Sieburg, H. & Moore, K. (2016), 'Hematopoietic stem cells count and remember self-renewal divisions', *Cell* **167**(5), 1296–1309.

Chambers, I., Silva, J., Colby, D., Nichols, J., Nijmeijer, B., Robertson, M., Vrana, J., Jones, K., Grotewold, L. & Smith, A. (2007), 'Nanog safeguards pluripotency and mediates germline development', *Nature* **450**(7173), 1230–1234.

Cook, D. (2016), *Practical machine learning with H2O: powerful, scalable techniques for deep learning and AI*, " O'Reilly Media, Inc.".

Dorshkind, K., Höfer, T., Montecino-Rodriguez, E., Pioli, P. D. & Rodewald, H.-R. (2019), 'Do haematopoietic stem cells age?', *Nature Reviews Immunology* pp. 1–7.

Dykstra, B., Olthof, S., Schreuder, J., Ritsema, M. & de Haan, G. (2011), 'Clonal analysis reveals multiple functional defects of aged murine hematopoietic stem cells', *Journal of Experimental Medicine* **208**(13), 2691–2703.

Ermolaeva, M., Neri, F., Ori, A. & Rudolph, K. L. (2018), 'Cellular and epigenetic drivers of stem cell ageing', *Nature Reviews Molecular Cell Biology* **19**(9), 594.

Florian, M. C., Dörr, K., Niebel, A., Daria, D., Schrezenmeier, H., Rojewski, M., Filippi, M.-D., Hasenberg, A., Gunzer, M., Scharffetter-Kochanek, K., Zheng, Y. & Geiger, H. (2012), 'Cdc42 activity regulates hematopoietic stem cell aging and rejuvenation', *Cell stem cell* **10**(5), 520–530.

Florian, M. C., Klose, M., Sacma, M., Jablanovic, J., Knudson, L., Nattamai, K. J., Marka, G., Vollmer, A., Soller, K., Sakk, V. et al. (2018), 'Aging alters the epigenetic asymmetry of hsc division', *PLoS biology* **16**(9), e2003389.

Foudi, A., Hochedlinger, K., Van Buren, D., Schindler, J. W., Jaenisch, R., Carey, V. & Hock, H. (2009), 'Analysis of histone 2b-gfp retention reveals slowly cycling hematopoietic stem cells', *Nature Biotechnology* **27**(1), 84.

Frede, J., Greulich, P., Nagy, T., Simons, B. D. & Jones, P. H. (2016), 'A single dividing cell population with imbalanced fate drives oesophageal tumour growth', *Nature cell biology* **18**(9), 967.

Friedman, J., Hastie, T. & Tibshirani, R. (2001), *The elements of statistical learning*, Springer series in statistics New York, NY, USA:.

García, P., Clarke, M., Vegiopoulos, A., Berlanga, O., Camelo, A., Lorvellec, M. & Frampton, J. (2009), 'Reduced c-myb activity compromises hscs and leads to a myeloproliferation with a novel stem cell basis', *The EMBO journal* **28**(10), 1492–1504.

Geiger, H., De Haan, G. & Florian, M. C. (2013), 'The ageing haematopoietic stem cell compartment', *Nature Reviews Immunology* **13**(5), nri3433.

Gilbert, P. M., Havenstrite, K. L., Magnusson, K. E., Sacco, A., Leonardi, N. A., Kraft, P., Nguyen, N. K., Thrun, S., Lutolf, M. P. & Blau, H. M. (2010), 'Substrate elasticity regulates skeletal muscle stem cell self-renewal in culture', *Science* **329**(5995), 1078–1081.

Gobaa, S., Hoehnel, S., Roccio, M., Negro, A., Kobel, S. & Lutolf, M. P. (2011), 'Artificial niche microarrays for probing single stem cell fate in high throughput', *Nature methods* **8**(11), 949.

Goodfellow, I., Bengio, Y., Courville, A. & Bengio, Y. (2016), *Deep learning*, Vol. 1, MIT press Cambridge.

Gower, J. (1974), 'Algorithm as 78: The mediancentre', *J R Statist Soc C* **23**(3), 466–470.

Grinenko, T., Eugster, A., Thielecke, L., Ramasz, B., Krüger, A., Dietz, S., Glauche, I., Gerbaulet, A., Von Bonin, M., Basak, O. et al. (2018), 'Hematopoietic stem cells can differentiate into restricted myeloid progenitors before cell division in mice', *Nature communications* **9**(1), 1–10.

Guidi, N., Sacma, M., Ständker, L., Soller, K., Marka, G., Eiwen, K., Weiss, J. M., Kirchhoff, F., Weil, T., Cancelas, J. A., Florian, M. C. & Geiger, H. (2017), 'Osteopontin attenuates aging-associated phenotypes of hematopoietic stem cells', *The EMBO journal* **36**(7), 840–853.

Harley, C. B., Futcher, A. B. & Greider, C. W. (1990), 'Telomeres shorten during ageing of human fibroblasts', *Nature* **345**(6274), 458.

Hato, T., Kimura, Y., Morisada, T., Koh, G. Y., Miyata, K., Tabata, M., Kadomatsu, T., Endo, M., Urano, T., Arai, F. et al. (2009), 'Angiopoietins contribute to lung development by regulating pulmonary vascular network formation', *Biochemical and biophysical research communications* **381**(2), 218–223.

Hills, M., Lücke, K., Chavez, E. A., Eaves, C. J. & Lansdorp, P. M. (2009), 'Probing the mitotic history and developmental stage of hematopoietic cells using single telomere length analysis (STELA)', *Blood* **113**(23), 5765–5775.

Ho, Y.-H. & Méndez-Ferrer, S. (2020), 'Microenvironmental contributions to hematopoietic stem cell aging', *haematologica* **105**(1), 38–46.

Hu, Y. & Smyth, G. K. (2009), 'Elda: extreme limiting dilution analysis for comparing depleted and enriched populations in stem cell and other assays', *Journal of immunological methods* **347**(1-2), 70–78.

Huang, D. W., Sherman, B. T. & Lempicki, R. A. (2008), 'Systematic and integrative analysis of large gene lists using david bioinformatics resources', *Nature protocols* **4**(1), 44.

Insinga, A., Cicalese, A., Faretta, M., Gallo, B., Albano, L., Ronzoni, S., Furia, L., Viale, A. & Pelicci, P. G. (2013), 'Dna damage in stem cells activates p21, inhibits p53, and induces symmetric self-renewing divisions', *Proceedings of the National Academy of Sciences* **110**(10), 3931–3936.

Ito, K., Bernardi, R., Morotti, A., Matsuoka, S., Saglio, G., Ikeda, Y., Rosenblatt, J., Avigan, D. E., Teruya-Feldstein, J. & Pandolfi, P. P. (2008), 'Pml targeting eradicates quiescent leukaemia-initiating cells', *Nature* **453**(7198), 1072–1078.

Ito, K. & Suda, T. (2014), 'Metabolic requirements for the maintenance of self-renewing stem cells', *Nature reviews Molecular cell biology* **15**(4), 243.

Karigane, D., Kobayashi, H., Morikawa, T., Ootomo, Y., Sakai, M., Nagamatsu, G., Kubota, Y., Goda, N., Matsumoto, M., Nishimura, E. K. et al. (2016), 'p38α activates purine metabolism to initiate hematopoietic stem/progenitor cell cycling in response to stress', *Cell Stem Cell* **19**(2), 192–204.

Kataoka, K., Sato, T., Yoshimi, A., Goyama, S., Tsuruta, T., Kobayashi, H., Shimabe, M., Arai, S., Nakagawa, M., Imai, Y. et al. (2011), 'Evi1 is essential for hematopoietic stem cell self-renewal, and its expression marks hematopoietic cells with long-term multilineage repopulating activity', *Journal of Experimental Medicine* **208**(12), 2403–2416.

Kiel, M. J., Yilmaz, Ö. H., Iwashita, T., Yilmaz, O. H., Terhorst, C. & Morrison, S. J. (2005), 'Slam family receptors distinguish hematopoietic stem and progenitor cells and reveal endothelial niches for stem cells', *cell* **121**(7), 1109–1121.

Loeffler, D., Wehling, A., Schneiter, F., Zhang, Y., Müller-Bötticher, N., Hoppe, P. S., Hilsenbeck, O., Kokkaliaris, K. D., Endele, M. & Schroeder, T. (2019), 'Asymmetric lysosome inheritance predicts activation of haematopoietic stem cells', *Nature* **573**(7774), 426–429.

Lutolf, M. P., Doyonnas, R., Havenstrite, K., Koleckar, K. & Blau, H. M. (2009), 'Perturbation of single hematopoietic stem cell fates in artificial niches', *Integrative biology* **1**(1), 59–69.

Matthews, W., Jordan, C. T., Wiegand, G. W., Pardoll, D. & Lemischka, I. R. (1991), 'A receptor tyrosine kinase specific to hematopoietic stem and progenitor cell-enriched populations', *Cell* **65**(7), 1143–1152.

McDavid, A., Finak, G., Chattopadyay, P. K., Dominguez, M., Lamoreaux, L., Ma, S. S., Roederer, M. & Gottardo, R. (2013), 'Data exploration, quality control and testing in single-cell qpcr-based gene expression experiments', *Bioinformatics* **29**(4), 461–467.

Mejia-Ramirez, E. & Florian, M. C. (2020), 'Understanding intrinsic hematopoietic stem cell aging', *haematologica* **105**(1), 22–37.

Mendelson, A. & Frenette, P. S. (2014), 'Hematopoietic stem cell niche maintenance during homeostasis and regeneration', *Nature medicine* **20**(8), 833.

Moore, K. A. & Lemischka, I. R. (2006), 'Stem cells and their niches', *Science* **311**(5769), 1880–1885.

Morrison, S. J. & Kimble, J. (2006), 'Asymmetric and symmetric stem-cell divisions in development and cancer', *nature* **441**(7097), 1068.

Morrison, S. J., Wandycz, A. M., Akashi, K., Globerson, A. & Weissman, I. L. (1996), 'The aging of hematopoietic stem cells', *Nature medicine* **2**(9), 1011.

Nakahara, F., Borger, D. K., Wei, Q., Pinho, S., Maryanovich, M., Zahalka, A. H., Suzuki, M., Cruz, C. D., Wang, Z., Xu, C., E, B. P., Ma'ayan, A., Greally, J. M. & Frenette, P. S. (2019), 'Engineering a haematopoietic stem cell niche by revitalizing mesenchymal stromal cells', *Nature cell biology* **21**(5), 560–567.

Nakahara, F., Weiss, C. N. & Ito, K. (2014), 'The role of pml in hematopoietic and leukemic stem cell maintenance', *International journal of hematology* **100**(1), 18–26.

Nichols, J., Zevnik, B., Anastassiadis, K., Niwa, H., Klewe-Nebenius, D., Chambers, I., Schöler, H. & Smith, A. (1998), 'Formation of pluripotent stem cells in the mammalian embryo depends on the pou transcription factor oct4', *Cell* **95**(3), 379–391.

Norddahl, G. L., Pronk, C. J., Wahlestedt, M., Sten, G., Nygren, J. M., Ugale, A., Sigvardsson, M. & Bryder, D. (2011), 'Accumulating mitochondrial dna mutations drive premature hematopoietic aging phenotypes distinct from physiological stem cell aging', *Cell stem cell* **8**(5), 499–510.

Notaro, R., Cimmino, A., Tabarini, D., Rotoli, B. & Luzzatto, L. (1997), 'In vivo telomere dynamics of human hematopoietic stem cells', *Proceedings of the National Academy of Sciences* **94**(25), 13782–13785.

Nygren, J. M. & Bryder, D. (2008), 'A novel assay to trace proliferation history in vivo reveals that enhanced divisional kinetics accompany loss of hematopoietic stem cell self-renewal', *PLoS One* **3**(11), e3710.

Opferman, J. T., Iwasaki, H., Ong, C. C., Suh, H., Mizuno, S.-i., Akashi, K. & Korsmeyer, S. J. (2005), 'Obligate role of anti-apoptotic mcl-1 in the survival of hematopoietic stem cells', *Science* **307**(5712), 1101–1104.

Orkin, S. H. & Zon, L. I. (2008), 'Hematopoiesis: an evolving paradigm for stem cell biology', *Cell* **132**(4), 631–644.

Pang, W. W., Price, E. A., Sahoo, D., Beerman, I., Maloney, W. J., Rossi, D. J., Schrier, S. L. & Weissman, I. L. (2011), 'Human bone marrow hematopoietic stem cells are increased in frequency and myeloid-biased with age', *Proceedings of the National Academy of Sciences* **108**(50), 20012–20017.

Perry, J. M., He, X. C., Sugimura, R., Grindley, J. C., Haug, J. S., Ding, S. & Li, L. (2011), 'Cooperation between both wnt/β-catenin and pten/pi3k/akt signaling promotes primitive hematopoietic stem cell self-renewal and expansion', *Genes & development* **25**(18), 1928–1942.

Prendergast, Á. M. & Essers, M. A. (2014), 'Hematopoietic stem cells, infection, and the niche', *Annals of the New York Academy of Sciences* **1310**(1), 51–57.

Qiu, J., Papatsenko, D., Niu, X., Schaniel, C. & Moore, K. (2014), 'Divisional history and hematopoietic stem cell function during homeostasis', *Stem Cell Reports* **2**(4), 473–490.

Ribeiro, M. T., Singh, S. & Guestrin, C. (2016), 'why should i trust you?' explaining the predictions of any classifier, *in* 'Proceedings of the 22nd ACM SIGKDD international conference on knowledge discovery and data mining', pp. 1135–1144.

Ritchie, M. E., Phipson, B., Wu, D., Hu, Y., Law, C. W., Shi, W. & Smyth, G. K. (2015), 'limma powers differential expression analyses for rna-sequencing and microarray studies', *Nucleic acids research* **43**(7), e47–e47.

Roch, A., Giger, S., Girotra, M., Campos, V., Vannini, N., Naveiras, O., Gobaa, S. & Lutolf, M. P. (2017), 'Single-cell analyses identify bioengineered niches for enhanced maintenance of hematopoietic stem cells', *Nature communications* **8**(1), 221.

Rossi, D. J., Bryder, D., Seita, J., Nussenzweig, A., Hoeijmakers, J. & Weissman, I. L. (2007), 'Deficiencies in dna damage repair limit the function of haematopoietic stem cells with age', *Nature* **447**(7145), 725–729.

Rossi, D. J., Bryder, D., Zahn, J. M., Ahlenius, H., Sonu, R., Wagers, A. J. & Weissman, I. L. (2005), 'Cell intrinsic alterations underlie hematopoietic stem cell aging', *Proceedings of the National Academy of Sciences* **102**(26), 9194–9199.

Saçma, M., Pospiech, J., Bogeska, R., de Back, W., Mallm, J.-P., Sakk, V., Soller, K., Marka, G., Vollmer, A., Karns, R., Cabezas-Wallscheid, N., Trumpp, A., Mendez-Ferrer, S., Milsom, M. D., Mulaw, M. A., Geiger, H. & Florian, M. C. (2019), 'Haematopoietic stem cells in perisinusoidal niches are protected from ageing', *Nature cell biology* **21**(11), 1309–1320. Indicate that quiescent HSCs in old mice localise to perisinusoidal niche. Niche cells inhibit HSC proliferation via Jag2.

Sakamoto, H., Takeda, N., Arai, F., Hosokawa, K., Garcia, P., Suda, T., Frampton, J. & Ogawa, M. (2015), 'Determining c-m yb protein levels can isolate functional hematopoietic stem cell subtypes', *Stem Cells* **33**(2), 479–490.

Säwén, P., Lang, S., Mandal, P., Rossi, D. J., Soneji, S. & Bryder, D. (2016), 'Mitotic history reveals distinct stem cell populations and their contributions to hematopoiesis', *Cell reports* **14**(12), 2809–2818.

Sharpless, N. E. & DePinho, R. A. (2007), 'How stem cells age and why this makes us grow old', *Nature reviews Molecular cell biology* **8**(9), 703–713.

Simons, B. D. & Clevers, H. (2011), 'Strategies for homeostatic stem cell self-renewal in adult tissues', *Cell* **145**(6), 851–862.

Stiehl, T. & Marciniak-Czochra, A. (2017), 'Stem cell self-renewal in regeneration and cancer: insights from mathematical modeling', *Current Opinion in Systems Biology* .

Sudo, K., Ema, H., Morita, Y. & Nakauchi, H. (2000), 'Age-associated characteristics of murine hematopoietic stem cells', *Journal of Experimental Medicine* **192**(9), 1273–1280.

Sugimura, R., He, X. C., Venkatraman, A., Arai, F., Box, A., Semerad, C., Haug, J. S., Peng, L., Zhong, X.-b., Suda, T. et al. (2012), 'Noncanonical wnt signaling maintains hematopoietic stem cells in the niche', *Cell* **150**(2), 351–365.

Sun, D., Luo, M., Jeong, M., Rodriguez, B., Xia, Z., Hannah, R., Wang, H., Le, T., Faull, K. F., Chen, R. et al. (2014), 'Epigenomic profiling of young and aged hscs reveals concerted changes during aging that reinforce self-renewal', *Cell stem cell* **14**(5), 673–688.

Takizawa, H., Regoes, R. R., Boddupalli, C. S., Bonhoeffer, S. & Manz, M. G. (2011), 'Dynamic variation in cycling of hematopoietic stem cells in steady state and inflammation', *Journal of Experimental Medicine* **208**(2), 273–284.

Thorén, L. A., Liuba, K., Bryder, D., Nygren, J. M., Jensen, C. T., Qian, H., Antonchuk, J. & Jacobsen, S.-E. W. (2008), 'Kit regulates maintenance of quiescent hematopoietic stem cells', *The Journal of Immunology* **180**(4), 2045–2053.

Trumpp, A., Essers, M. & Wilson, A. (2010), 'Awakening dormant haematopoietic stem cells', *Nature Reviews Immunology* **10**(3), 201.

Van Der Maaten, L., Postma, E. & Van den Herik, J. (2009), 'Dimensionality reduction: a comparative', *J Mach Learn Res* **10**, 66–71.

van Galen, P., Kreso, A., Mbong, N., Kent, D. G., Fitzmaurice, T., Chambers, J. E., Xie, S., Laurenti, E., Hermans, K., Eppert, K. et al. (2014), 'The unfolded protein response governs integrity of the haematopoietic stem-cell pool during stress', *Nature* **510**(7504), 268.

Van Kampen, N. G. (1992), *Stochastic processes in physics and chemistry*, Vol. 1, Elsevier.

Van Valen, L. (2005), Chapter 3 - The Statistics of Variation, *in* B. Hallgrímsson & B. K. Hall, eds, 'Variation', Academic Press, Burlington, pp. 29–47.

Walter, D., Lier, A., Geiselhart, A., Thalheimer, F. B., Huntscha, S., Sobotta, M. C., Moehrle, B., Brocks, D., Bayindir, I., Kaschutnig, P. et al. (2015), 'Exit from dormancy provokes DNA-damage-induced attrition in haematopoietic stem cells', *Nature* **520**(7548), 549.

Werner, B., Beier, F., Hummel, S., Balabanov, S., Lassay, L., Orlikowsky, T., Dingli, D., Brümmendorf, T. H. & Traulsen, A. (2015), 'Reconstructing the in vivo dynamics of hematopoietic stem cells from telomere length distributions', *Elife* **4**, e08687.

Wilson, A., Laurenti, E., Oser, G., van der Wath, R. C., Blanco-Bose, W., Jaworski, M., Offner, S., Dunant, C. F., Eshkind, L., Bockamp, E. et al. (2008), 'Hematopoietic stem cells reversibly switch from dormancy to self-renewal during homeostasis and repair', *Cell* **135**(6), 1118–1129.

Wilson, A. & Trumpp, A. (2006), 'Bone-marrow haematopoietic-stem-cell niches', *Nature Reviews Immunology* **6**(2), 93.

Wu, M., Kwon, H. Y., Rattis, F., Blum, J., Zhao, C., Ashkenazi, R., Jackson, T. L., Gaiano, N., Oliver, T. & Reya, T. (2007), 'Imaging hematopoietic precursor division in real time', *Cell stem cell* **1**(5), 541–554.

Yamashita, Y. M., Yuan, H., Cheng, J. & Hunt, A. J. (2010), 'Polarity in stem cell division: asymmetric stem cell division in tissue homeostasis', *Cold Spring Harbor perspectives in biology* **2**(1), a001313.

Yilmaz, Ö. H., Valdez, R., Theisen, B. K., Guo, W., Ferguson, D. O., Wu, H. & Morrison, S. J. (2006), 'Pten dependence distinguishes haematopoietic stem cells from leukaemia-initiating cells', *Nature* **441**(7092), 475.

Zhang, J., Grindley, J. C., Yin, T., Jayasinghe, S., He, X. C., Ross, J. T., Haug, J. S., Rupp, D., Porter-Westpfahl, K. S., Wiedemann, L. M. et al. (2006), 'Pten maintains haematopoietic stem cells and acts in lineage choice and leukaemia prevention', *Nature* **441**(7092), 518–522.

Zhang, Z., Huang, Z., Ong, B., Sahu, C., Zeng, H. & Ruan, H.-B. (2019), 'Bone marrow adipose tissue-derived stem cell factor mediates metabolic regulation of hematopoiesis', *haematologica* **104**(9), 1731–1743.

Zimdahl, B., Ito, T., Blevins, A., Bajaj, J., Konuma, T., Weeks, J., Koechlein, C. S., Kwon, H. Y., Arami, O., Rizzieri, D. et al. (2014), 'Lis1 regulates asymmetric division in hematopoietic stem cells and in leukemia', *Nature genetics* **46**(3), 245.

STAR METHODS

CONTACT FOR REAGENT RESOURCE SHARING

Further information an requests for resources should be directed and will be fulfilled by the Lead Contact, Ben MacArthur (bdm@soton.ac.uk).

Materials Availability

This study did not generate new materials.

Data and Code Availability

Source data statement: source data have been deposited at ArrayExpress and are publicly available under the accession numbers E-MTAB-7504 and E-MTAB-7321.

Code statement: Original code is publicly available at https://github.com/passt/hsc-division-patterns.

Scripts statement: The scripts used to generate the figures reported in this paper are available in the R package and their use is described in the **STAR Methods**.

Any additional information required to reproduce this work is available from the Lead Contact.

EXPERIMENTAL MODEL AND SUBJECT DETAILS

Mice and cells

C57BL/6 (B6-Ly5.2), C57BL/6 mice congenic for the Ly5 locus (B6-Ly5.1) were purchased from Sankyo-Lab Service (Tsukuba, Japan). Evi1-GFP knock-in mice were provided by Dr. Kurokawa (The University of Tokyo, Japan). Mice expressing Cre recombinase under the control of the Type I collagen (Col1a1) promoter (Col1a1-Cre) and inducible Angpt1 transgenic (CAGp-IND-COMP-Angpt1 Tg) mice (Hato et al. 2009) were used to obtain constant and specific expression of Angpt1 in osteoblasts (Col1a1-Cre(+): Angpt1 Tg). The gene recombination experiment safety and animal experiment committees at Keio and Kyushu Universities approved this study, and all experiments were carried out in accordance with the guidelines for animal and recombinant DNA experiments at both Universities.

METHOD DETAILS

Flow cytometry and antibodies

The following monoclonal antibodies (Abs) were used for flow cytometry and cell sorting: anti-c-Kit (2B8, BD Biosciences, 1:100), -Sca-1 (E13-161.7, BD Biosciences, 1:100), -CD4 (RM4-5, BD Biosciences, 1:100), -CD8 (53-6.7, BD Biosciences, 1:100), -B220 (RA3-6B2, BD Biosciences, 1:100), -TER-119 (BD Biosciences, 1:100), -Gr-1 (RB6-8C5, BD Biosciences, 1:100), -Mac-1 (M1/70, BD Biosciences, 1:100), -CD41 (MWReg30, eBioscience, 1:100), -CD48 (HM48-1, Biolegend, 1:100), -CD150 (TC15-12F12.2, Biolegend, 1:100), -CD34 (RAM34, BD Biosciences, 1:20), -CD45.1 (A20, BD Biosciences, 1:100), -CD45.2 (104, BD Biosciences, 1:100), and -Tie2 (TEK4, eBioscience, 1:100). A mixture of CD4, CD8, B220, TER-119, Mac-1, and Gr-1 was used as the lineage mix. To isolate Evi1$^+$ LT-HSCs, Evi1-GFP mouse bone marrow (BM) cells were purified using a two-step protocol. First, LT-HSCs were enriched by positive selection for c-Kit expression using anti-CD117 immunomagnetic beads (130-091-224, Miltenyi Biotec Inc. 1:5 dilution). Second, c-Kit$^+$ enriched cells were stained with a set of fluorophore-conjugated antibodies (lineage mix, anti-Sca-1, anti-c-Kit, anti-CD48, anti-CD150, and anti-CD34). For the analysis of Tie2 expression, BM cells from Evi1-GFP mice were stained with the lineage mix, anti-Sca-1, anti-c-Kit, anti-CD48, anti-CD150, anti-CD34, and anti-Tie2 antibodies. Stained cells were analyzed and sorted by flow-cytometry using a FACS Aria III (BD Biosciences).

Microarrays

LSKCD41$^-$CD48$^-$CD150$^+$CD34$^+$ cells, LSKCD41$^-$CD48$^-$CD150$^+$CD34$^-$ Evi1-GFP$^-$ cells, and LSKCD41$^-$CD48$^-$CD150$^+$CD34$^-$ Evi1$^+$ cells were selected sorted from 8-week-old mice, and RNA was isolated from each population using an RNeasy Plus

Micro Kit (Qiagen) according to the manufacturer's instructions. RNA quality was confirmed with a 2100 Bioanalyzer (Agilent Technologies, Santa Clara, CA). Total RNA (1.5ng) was reverse transcribed and amplified using the Ovation Pico WTA System V2 (NuGEN) with Ribo-SPIA technology. Amplified cDNA (5μg) was fragmented and labeled with biotin using Encore Biotin Module (NuGEN), and hybridized to a GeneChip Mouse Genome 430 2.0 Array (Affymetrix) according to the manufacturer's instructions. All hybridized microarrays were scanned using a GeneChip Scanner (Affymetrix). Relative hybridization intensities and background hybridization values were calculated using the Affymetrix Expression Console software (Affymetrix). Raw signal intensities for each probe were calculated from hybridization intensities. Raw signal intensities were normalized using the MAS5 method.

Paired daughter cell assay

Individual Evi1$^+$ LT-HSCs were selected from 4-week-old, 8-week-old, and 18-month-old mice and directly sorted (one-per-well) into fibronectin-coated 96 well U-bottom plates. Cells were cultured in SF-O3 medium in the presence of 0.1% BSA, 100 ng/ml SCF, and 100 ng/ml TPO with or without Angpt1 (1 μg/ml, a gift from Dr. Koh, Korea Advanced Institute of Science and Technology). After 2 days of culture, daughter cells derived from single Evi1$^+$ LT-HSCs were separated using a micro-manipulator (NARISHIGE, Japan) and transferred one-per-well to PCR plates containing a mixture of CellsDirect 2$\times$ Reaction Mix (Invitrogen), pooled 0.2$\times$ TaqMan Gene Expression Assays, and SuperScript III RT/Platinum Taq Mix (Invitrogen). Reverse transcription (RT) (at 50°C for 15 min), an initial denature step (95°C for 2min), and specific target amplification (STA) (22 cycles of 15s at 95°C alternating with 1 min at 60°C) were performed sequentially. Pre-amplified cDNA was diluted with TE buffer (1:5). Gene expression read-out was performed using BioMark 96·96 Dynamic Array and BioMark system (Fluidigm) according to manufacturer's instructions. TaqMan Gene Expression Assays used in this study are listed in **Supplemental Table S1**.

Training data for classifier

To prepare the training data needed for our artificial neural network classifier, we profiled the expression of the same set of 96 HSC-related genes that we used in the PDC assay (see **Supplemental Table S1**) in 96 individual cells isolated without culture from the following nine populations:

1. LSKCD41$^+$CD48$^+$CD150$^+$ progenitor cells taken from 4-week-old mice (designated week 4 CD150$^+$)
2. LSKCD41$^+$CD48$^+$CD150$^-$ progenitor cells taken from 4-week-old mice (designated week 4 CD150$^-$)
3. LSKCD41$^-$CD48$^-$CD150$^+$ Evi1$^+$ stem cells taken from 4-week-old mice (designated week 4 Evi1$^+$)
4. LSKCD41$^-$CD48$^-$CD150$^-$CD34$^+$ progenitor cells taken from 8-week-old mice (designated week 8 CD150$^-$)
5. LSK progenitor cells taken from 8-week-old mice (designated week 8 LSK)
6. LSKCD41$^-$CD48$^-$CD150$^+$CD34$^-$ Evi1$^+$ taken from 8-week-old mice (designated week 8 Evi1$^+$)
7. LSKCD41$^-$CD48$^-$CD150$^-$CD34$^+$ progenitor cells taken from 18-month-old mice (designated 18 month CD150$^-$)
8. LSKCD41$^+$CD48$^+$CD150$^+$CD34$^+$ progenitor cells taken from 18-month-old mice (designated 18 month CD150$^+$)
9. LSKCD41$^-$CD48$^-$CD150$^+$CD34$^-$ Evi1$^+$ stem cells taken from 18-month-old mice (designated 18 month Evi1$^+$)

Individual cells from each population were sorted directly into a mixture of CellsDirect 2$\times$ Reaction Mix, pooled 0.2$\times$ TaqMan Gene Expression Assays, and SuperScript III RT/Platinum Taq Mix. Following RT-STA (described above), gene expression was then analyzed using BioMark 96·96 Dynamic Arrays (Fluidigm). In all cases training samples were taken from a pool of cells from at least three distinct mice.

Bone marrow transplantation

To evaluate the number of LT-HSCs, Ly5.1$^+$ LSKCD41$^-$CD48$^-$CD150$^+$CD34$^-$Evi1-GFP$^-$ and -Evi1$^+$ cells were transplanted into lethally irradiated Ly5.2$^+$ mice using 2×10^5 competitor cells. The percentage of donor-derived cells in PB was analyzed monthly by flow cytometry. To evaluate the effect of the Angpt1 on the regulation of LT-HSC number in vivo, LSKCD48$^-$ cells were isolated from Col1a1-Cre(+);Angpt1(+) Tg mice or Col1a1-Cre(–);Angpt1(+) control mice and the limiting number of cells (20, 30, 40, and 50 cells for Angpt1 Tg mice, 50, 75, and 100 cells for control mice) were transplanted into lethally irradiated recipient mice with 2×10^5 competitor cells. The percentages of donor-derived cells were analyzed 4 months after BMT. PB chimerism of $> 1.0\%$ at 16 weeks after BMT was taken to verify long-term engraftment. To investigate the effect of Angpt1 in the maintenance of LT-HSC number *in vitro*, PDCs derived from control culture or Angpt1 supplemented culture were were pooled and 1, 2, 3, 4, and 6 pairs of PDCs from the pooled samples were transplanted into lethally irradiated recipient mice with 2×10^5 competitor cells. The percentages of donor-derived cells were analyzed 4 months after BMT. PB chimerism of $> 0.3\%$ at 16 weeks after BMT was taken to verify long-term engraftment. The frequency of LT-HSCs and statistical significance were determined using the ELDA software (Hu & Smyth 2009).

Manufacture of poly(ethylene glycol) (PEG) microwells

PEG-based hydrogel microwells were manufactured as previosuly described (Roch et al. 2017). Briefly, arrays of hydrogel microwells were fabricated using standard photolithography to etch the microwell pattern into a silicon substrate onto which liquid thermocurable poly(dimethylsiloxane) (PDMS) was polymerized. This template was then used to cast hydrophilic polymer precursors of PEG that were covalently crosslinked to form inert hydrogels. PEG hydrogel microwell arrays were then removed from the PDMS, equilibrated in PBS, and attached to the bottom of tissue culture wells.

QUANTIFICATION AND STATISTICAL ANALYSIS

Figure plots were produced in RStudio and MATLAB using default packages unless otherwise stated.

Microarray data analysis

Differentially expressed genes from microarray studies were determined using the R package limma (Ritchie et al. 2015). Genes withe FDR corrected p-values < 0.05 (see **Supplemental Table S2**) were used for gene set enrichment analysis using the biological processes Gene Ontology (GO) in DAVID (Huang et al. 2008).

Normalization and analysis of single-cell qRT-PCR data

Cycling threshold (CT) values ≥ 28 were considered absent. Raw CT values were normalized by subtracting the median CT values of loading control (*Gapdh*) from each reading on the array. Normalised CT values were then transformed linearly to expression threshold (ET) values ranging from 0 (absent) to 28 (maximum expression). Gene expression asymmetry for each given gene was assessed by comparing ET levels between daughter cells. Specifically, if g_{ij} denotes the ET level of gene g_i in daughter cell $j = 1,2$ then expression asymmetry is given by $a_i = |g_{i1} - g_{i2}|$. Total asymmetry for the division was then defined as $\sum_i a_i$.

Clustering and dimensionality reduction

All clustering and dimensionality reduction was performed in R (version 3.1.2 or later) and MATLAB® (The MathWorks Inc., Natick, MA, 2016, version 8.5 or later) using standard routines. Hierarchical clustering was performed in R using Euclidean distance and average linkage, t-distributed stochastic neighbour embedding (t-SNE) was performed in MATLAB® using the Toolbox for Dimensionality Reduction (Van Der Maaten et al. 2009) with default settings.

Estimation of dispersion

To the *i*th cell in the population we associate a gene expression vector $G_i = (g_1, g_2, \ldots, g_{96}) \in \mathbb{R}^{96}$, which records its expression status with respect to the 96 genes we measured. Assuming that there are n cells in the population, the mediancentre is that

point $M = (m_1, m_2, \ldots, m_{96}) \in \mathbb{R}^{96}$ such that $D = \sum_{i=1}^{n} d(G_i, M)$ is minimum, where $d(x,y) = \sum_{j=1}^{96} |x_j - y_j|$ is the L_1-distance. The mediancentre is a multivariate generalization of the univariate median (Gower 1974). The dispersion of the population is the minimized value of D. The dispersion is a simple statistic that can be used in hypothesis testing to compare the multivariate variability in different populations (Van Valen 2005).

Artificial neural network

We used a deep feedforward artificial neural network (ANN) to distinguish between the nine training samples, and thereby identify the regenerative status of the cell (stem or progenitor cell) and its age (4-week-old, 8-week-old or 18-month-old) directly from its transcriptional profile. Network parameters were optimized using grid search over a range of network architectures, including number of hidden layers and nodes per layer, activation functions and regularization regimes. We found that the ANN constructed with two hidden layers of 150 rectifying linear units (ReLUs) each, trained with cross-entropy loss function using dropout (20% dropout for input and 50% and 75% for the two hidden layers respectively) and additional L_1 and L_2 regularization (both with 0.002 penalty), with soft-max output performed best. For each set of network parameters optimization was performed with 10-fold cross-validation using stochastic gradient descent and back-propagation. All reported metrics refer to cross-validated results. All training and optimization was performed in R using the H2O deep learning library (Cook 2016).

Model analysis

We used LIME (Local Interpretable Model-agnostic Explanations) to explain the predictions of our ANN, and identify genes that had a significant role in deciding individual cell identities (Ribeiro et al. 2016). LIME explains the output of a machine learning model by approximating the (possibly highly nonlinear) model locally with a sparse interpretable model, from which feature importances can be assessed. To apply LIME to our data we used it to determine which genes were most important in classifying individual PDCs. Since PDCs were not assigned to all nine classes (defined above) equally we considered only those classes for which at least 50 PDCs were assigned (Week 4 Evi-1$^+$, week 4 CD150$^+$, Week 8 Evi-1$^+$, week 8 CD150$^-$ and 18 month CD150$^+$). For each represented class we selected a random sample of 25 PDCs assigned to that class by our ANN and used LIME to determine the ten genes that were most important in classifying each of the 25 cells. Subsequent analysis was not dependent on the 25 cells sampled. Important genes were identified using greedy forward selection based on a ridge regression fit to the ANN. To avoid inclusion of spurious features from local models that did well approximate the ANN, only models for which the coefficient of determination was greater than 0.1 were subsequently considered. Important regulators of each class were identified as those genes that were most important (i.e. in the top ten) in determining the identity of at least 50% of PDCs in that class. All calculations were performed using the LIME package in R (Ribeiro et al. 2016).

Mathematical Modeling

The simplest stochastic model of stem cell proliferation assumes the following set of events:

$$S \xrightarrow{k_1} S+S \qquad S \xrightarrow{k_2} S+P \qquad S \xrightarrow{k_3} P+P \tag{1}$$

where S denotes a stem cell and P denotes a progenitor. The first event is a symmetric S-S division, in which 2 stem cells are produced via division, resulting in a gain of one stem cell to the pool; the second is an asymmetric S-P division, in which one stem cell is produced via division, resulting in no change to the stem cell pool; and the third is a symmetric P-P division, resulting in a loss of one stem cell from the pool. Let $p_n(t)$ be the probability that there are n stem cells in the pool at time t. The master equation describing these dynamics is:

$$\frac{dp_n}{dt} = (n+1)k_3 p_{n+1} + (n-1)k_1 p_{n-1} - n(k_1+k_3)p_n. \tag{2}$$

Let $M(t) = \sum_n n p_n$ denote the expected number of stem cells in the pool at time t. The equation for $M(t)$ may easily be found to be (Van Kampen 1992):

$$\frac{dM}{dt} = (k_1 - k_3)M, \tag{3}$$

from which we obtain, $M = M(0)\exp([k_1 - k_3]t)$. Assuming that the cell cycle time is constant, we may write $k_1 = pk$ and $k_3 = qk$, where $\log(2)/k$ is the cell cycle time, p is the probability that an S-S division occurs and q is the probability that a P-P division occurs. Thus, $M = M(0)\exp(k\Delta t)$, where $\Delta = p - q$. If $\Delta > 0$ then S-S divisions are more likely than P-P divisions and the stem cell pool will expand, while if $\Delta < 0$ then P-P divisions are more likely than S-S divisions and the stem cell pool will deplete. If $\Delta = 0$ then S-S and P-P divisions are equiprobable, and homeostasis is maintained (i.e. $M(t) = M(t = 0)$ for all t).

Supplemental Figures

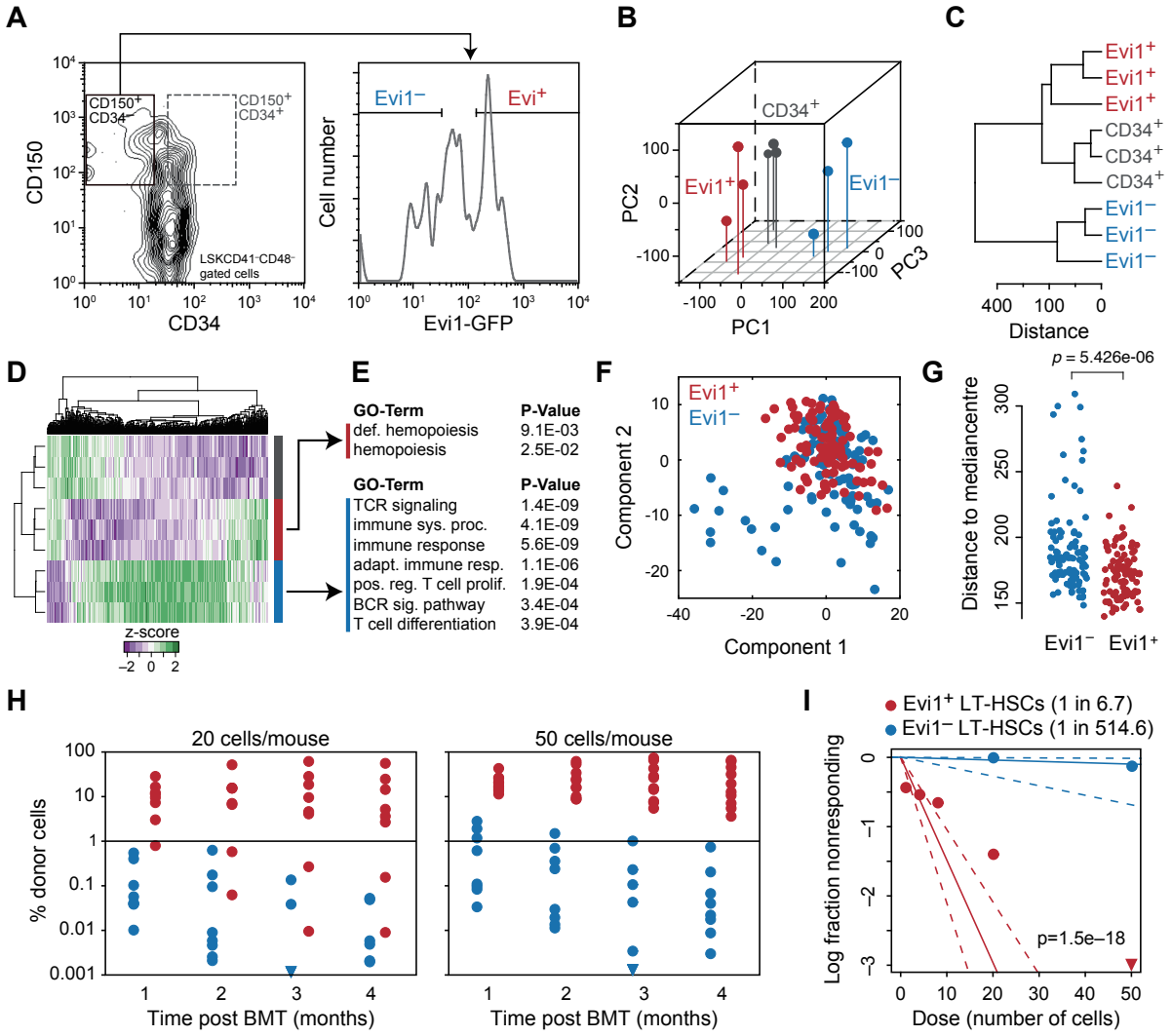

Figure S1. Evi1 expression is positively associated LT-HSC activity. (A) Selection protocol. LSKCD41$^-$CD48$^-$CD150$^+$CD34$^+$ (dotted square in panel A, denoted CD34$^+$), LSKCD41$^-$CD48$^-$CD150$^+$CD34$^-$ Evi1$^+$ (denoted Evi1$^+$) and LSKCD41$^-$CD48$^-$CD150$^+$CD34$^-$ Evi1$^-$ (denoted Evi1$^-$) fractions were isolated from the mouse BM. (B-E) CD150$^+$CD34$^+$, Evi1$^+$ and Evi1$^-$ fractions form distinct populations based upon global gene expression patterns as assessed by microarray (at least 4500 cells per sample were isolated for each cell type from 3 mice). (B) Projection of global expression patterns on to the first three principal components (PCs, three biological replicates per population). (C) Hierarchical clustering of global expression patterns (3 biological replicates per population). (D) Heatmap of global expression patterns shows that each population is characterized by different combinations of gene expression. (E) Genes associated with definitive hemopoiesis are upregulated in the Evi1$^+$ fraction; genes associated differentiation are upregulated in the Evi1$^-$ fraction. (F-G) Single cell qPCR profiling of Evi1$^{+/-}$ fractions (96·96 Dynamic Array, BioMark^{TM} system, Fluidigm). A detailed gene list and primers used are provided in the **Supplemental Table S1**. The Evi1$^+$ fraction is more homogeneous than the Evi1$^-$ fraction. (F) Projection of single cell expression patterns on to the first two Principal components. (G) distance to mediancentre as a measure of dispersion (see **STAR Methods**) in the Evi1$^+$ and Evi1$^-$ fractions. *p*-value is from two sided t-test (96 cells in each group). (H-I) Results of bone marrow transplantations. Evi1$^+$ cells show better engraftment as assessed by: (H) percentage donor derived cells in peripheral blood following competitive BMT and (I) enrichment for functional LT-HSCs from limiting dilution BMT. *p*-value is from extreme value limiting dilution analysis (ELDA) (Hu & Smyth 2009). The following number of mice (*n*) were used: *n* = 52: Evi1-GFP$^+$ 1 cell; *n* = 19, Evi1-GFP$^+$ 4 cells; *n* = 19, Evi1-GFP$^+$ 8 cells; *n* = 8, Evi1-GFP$^+$ 20 cells; *n* = 10, Evi1-GFP$^+$ 50 cells; *n* = 7, Evi1-GFP$^-$ 20 cells; *n* = 8, Evi1-GFP$^-$ 50 cells. In all panels data relates to cells taken from 8-week-old mice.

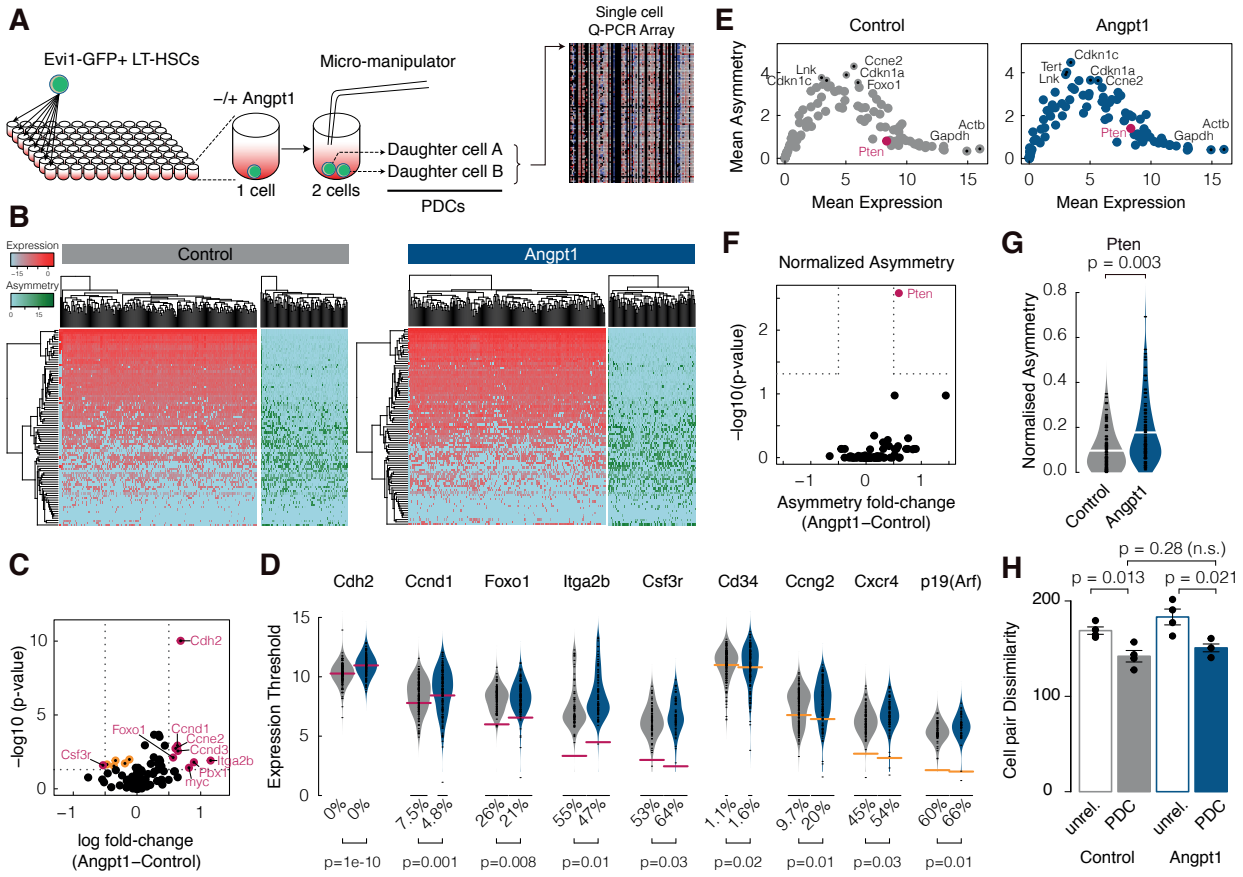

Figure S2. Angpt1 regulation of HSC dynamics is highly combinatorial. (A) Schematic of paired-daughter cell assay. Individual Evi1^{+} cells were seeded on to multi-well plates. Following cell division *in vitro*, daughter cells were manually separated and processed for gene expression analysis by qPCR array. (B) Heat-map of single-cell gene expression and asymmetry patterns (see **STAR Methods**) from control (left) and Angpt1 treated (right) cultures. Expression patterns are in red-blue, asymmetry patterns are in green-blue. Expression and asymmetry (see **STAR Methods**) patterns are variable in both conditions. (C-D) Angpt1 treatment significantly increased expression of cell adhesion molecules (such as *Cdh2, Itga2b*) responsible for HSC homing, as well as positive and negative regulators of the cell cycle (such as *Ccnd1, Ccnd3, Ccne1, Foxo1, Ccng2*). Angpt1 significantly reduced the expression of mobilization signal-receptors (such as *Csf3r, Cxcr4*) and mobilization indicators (such as *Cd34*) and senescence factors (such as *p19-Arf*).(C) Volcano-plot, showing the expression difference between treatment conditions (log-fold-change of mean) and negative log of *p*-values (FDR corrected using the Benjamni-Hochberg [BH] method) from a hypothesis test for single cell differential gene expression (McDavid et al. 2013). Significant genes (FDR corrected *p*-value < 0.05, and expected fold change > 1.4) are highlighted in cerise; orange points mark significant genes that do not meet the fold-change criterion. (D) Violin-plots of expression values in control (grey) and treatment (blue) conditions for selected genes. Values along the x-axis indicate the percentage of zero readings. Note that the percentage of zeros can vary substantially and thereby contribute considerably to statistical significance. Cerise and orange bars indicate expression mean, and fold-change levels from panel C. (E) Plots of mean expression against mean division asymmetry in control (left, grey) and Angpt1 treated (right, blue) LT-HSCs. Expression asymmetry has a nonlinear relationship to expression. Some key regulators are shown. F) Volcano-plot, showing the asymmetry difference between treatment conditions (log-fold-change of mean asymmetry) and negative log of *p*-values (FDR corrected using the BH method). Significant genes (FDR corrected *p*-value < 0.05, and fold change > 1.4) are highlighted in cerise. Only *Pten* a negative regulator of the PI3K-AKT signalling pathway that controls HSC proliferation, survival, differentiation, and migration (Yilmaz et al. 2006) was significantly differentially partitioned on Angpt1 treatment. (G) Violin-plot of expression asymmetry for *Pten*. *p*-value is from a Wilcoxon rank sum test (FDR corrected using BH method). White bar indicates median. (H) Dissimilarity of randomly selected daughter cell pairs (i.e. unrelated) and paired-daughter cells (PDCs) from the same division (see **STAR Methods**). PDCs tended to be more like each other than randomly selected pairs of unrelated cells from the daughter cell population. Data is presented as mean ± standard deviation, *p*-values are from two sided t-tests (from three biological replicates containing 48 pairs of cells each).

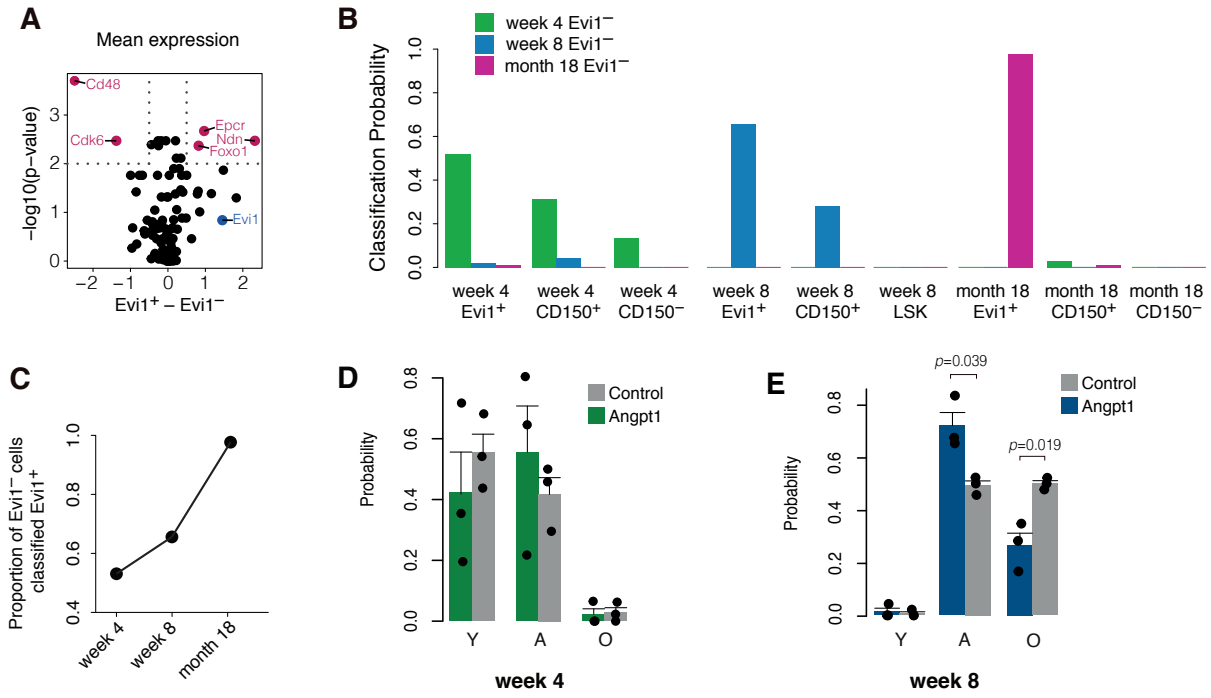

Figure S3. Single cell profiling of the Evi1$^-$ fraction. (A) Volcano-plot of single cell gene expression differences between the Evi1$^+$ and Evi1$^-$ fractions (log-fold-change of mean expression) and negative log of *p*-values (FDR corrected using the Benjamni-Hochberg [BH] method) from a hypothesis test for single cell differential gene expression (McDavid et al. 2013). Significant genes (FDR corrected p-value < 0.01, and fold change > 1.4) are highlighted in cerise; Evi1 (highlighted in blue) is substantially upregulated (fold-change > 2) in the Evi1$^+$ fraction, but does not pass the corrected significance threshold. (B) Results of classification of Evi1$^-$ cells using our ANN classifier. (C) The proportion of Evi1$^-$ cells classified as Evi1$^+$ increases with age, indicating that these two populations become more alike with age. (D-E) ANN predicted daughter cell characteristic ages from (D) young and (E) adult Evi1+ HSC divisions without regard for daughter cell pairings. Data from three biological replicates containing 48 pairs of cells each are shown.

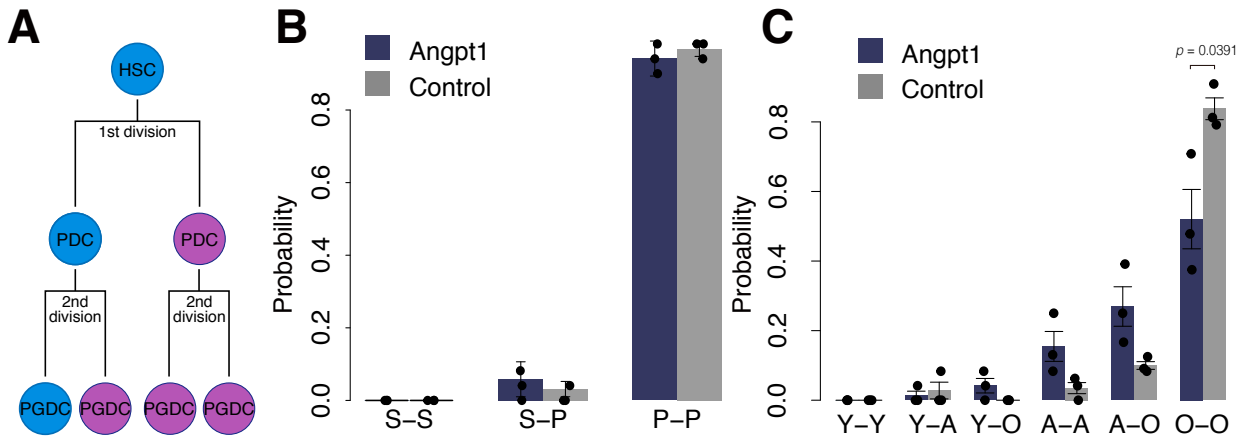

Figure S4. Comparison of paired granddaughter cells. (A) Schematic of the paired granddaughter (PGDC) cell assay, starting from a single 8-week-old HSC. (B) Classification of PGDC divisions using our trained ANN, restricted to regenerative status. Most secondary divisions in culture give rise to daughters with progenitor characteristics. (C) Classification of PGDC divisions using trained ANN, restricted to characteristic age. Spontaneous acquisition of age-associated characteristics is very commonly observed in one or other, or both, granddaughter cells. Spontaneous rejuvenation is never observed, to within accuracy of classifier. In all panels data are expressed as the mean ± the standard deviation. In all panels 48 pairs of cells were analyzed from pooled LT-HSC samples obtained from 3-4 experiments, each using 2-3 mice. *p*-value is from two sided t-test.

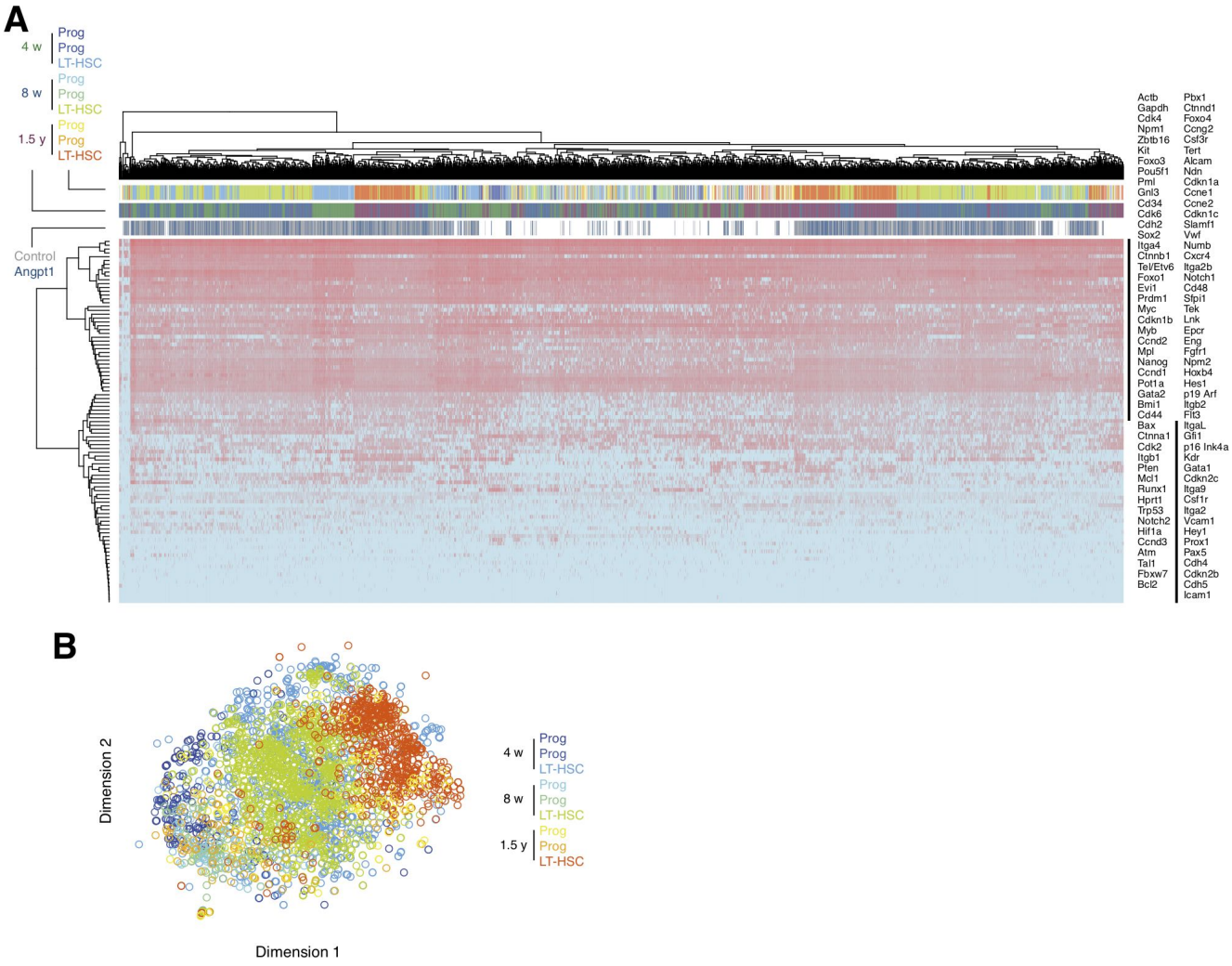

Figure S5. Heatmap and tSNE plot of combined data. (A) Heatmap and (B) tSNE plot showing the combined training and test data from mice of all ages and treatment conditions.

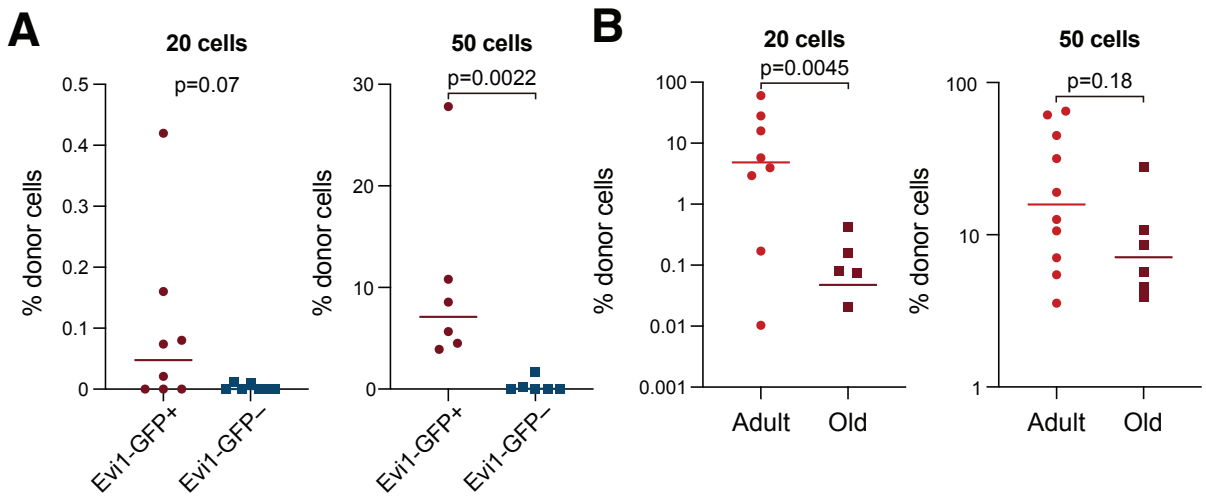

Figure S6. Bone marrow transplantation of old HSCs. (A) Evi1$^+$ LSKCD41$^-$CD48$^-$CD150$^+$CD34$^-$ HSCs taken from 18-month-old mice show better engraftment than Evi1$^-$ cells as assessed by percentage donor derived cells in peripheral blood. (B) Evi1$^+$ HSCs taken from 18-month-old mice show poorer engraftment than Evi1$^+$ HSCs taken from 8-week-old mice. *p*-values are from two-sided t-tests.

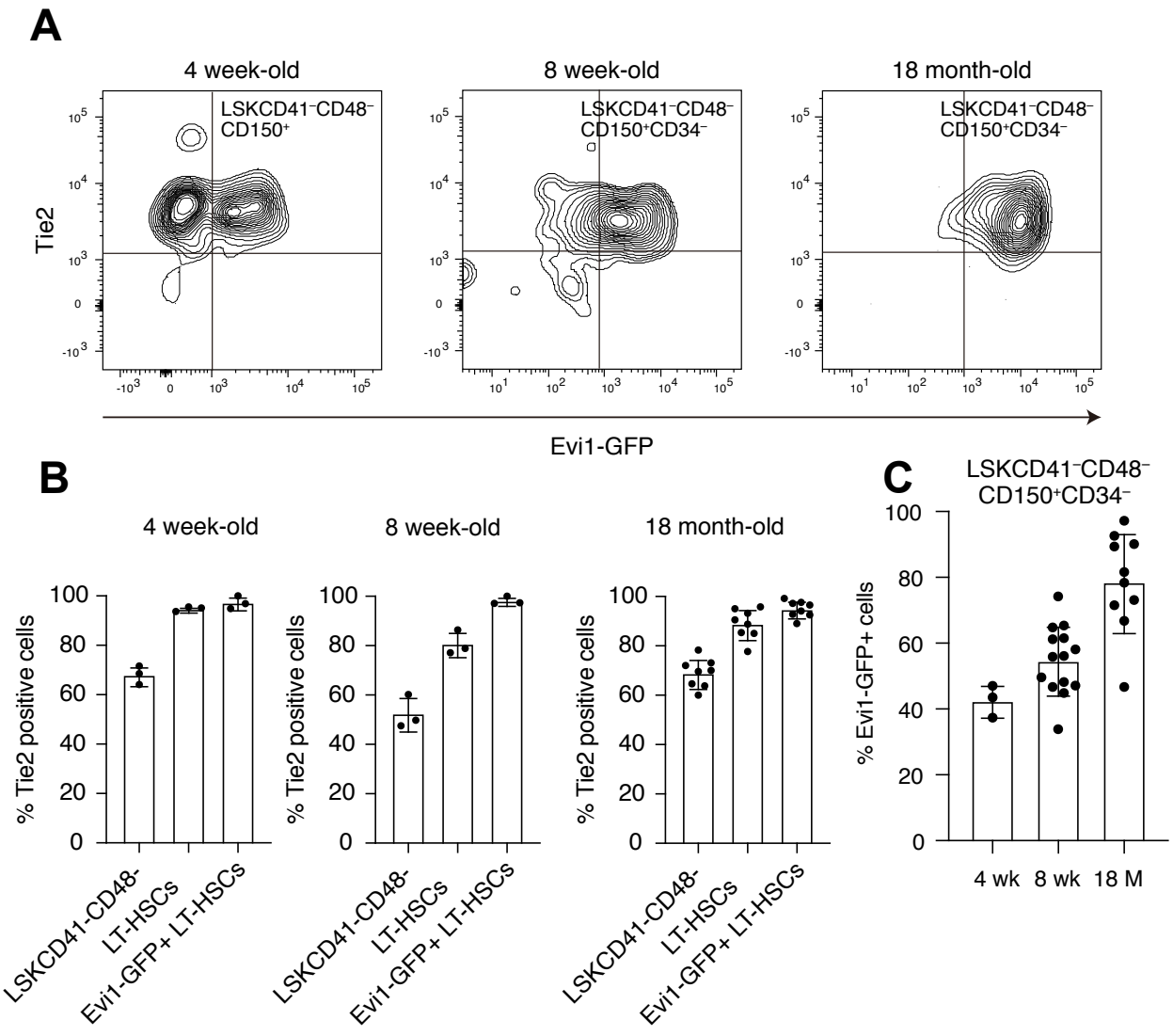

Figure S7. Angpt1 and Tie2 expression in young, adult and aged HSCs. (A) Coexpression patterns of Angpt1 and Tie2 throughout life. (B) LT-HSCs retain Tie2 expression with age. (C) The percentage of Evi1$^+$ cells within the LSKCD41$^-$CD48$^-$CD150$^+$CD34$^-$ fraction increases with age. In all panels data are expressed as the mean ± the standard deviation. Representative data from 3 independent experiments are shown.

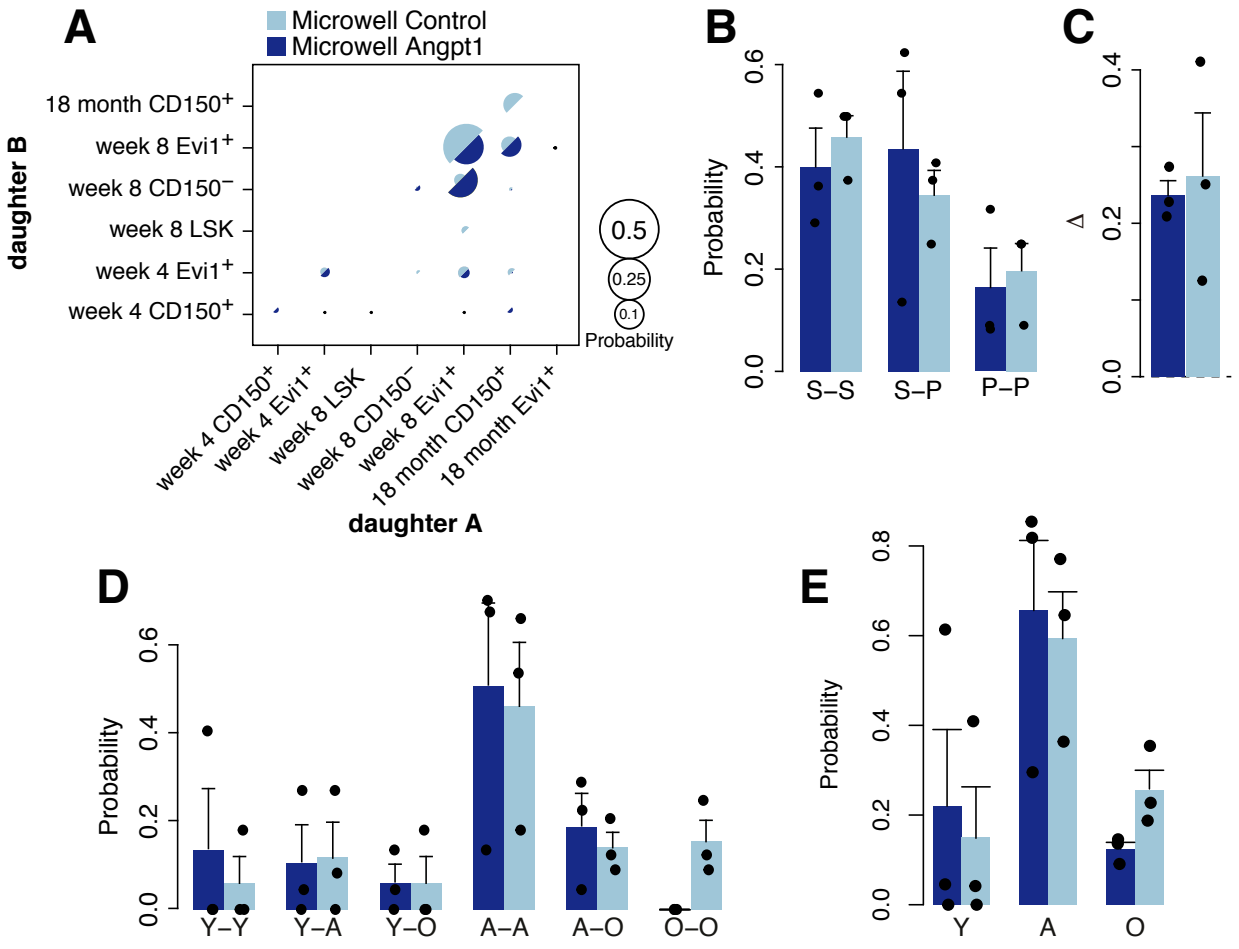

Figure S8. Division patterns of LT-HSCs cultured in PEG microwells. (A) Classification of divisions from adult (8-week-old) stem cells cultured in PEG microwells using trained ANN. Daughter cell identities are not ordered. (B) Classification restricted to regenerative status. A range of divisions is observed in both control and Angpt1 treated conditions. (C) The expansion factor Δ is positive in both control and Angpt1 treated conditions indicating robust expansion of the stem cell pool. (D) Classification restricted to characteristic age. Both daughter cells from the majority of divisions retain appropriate age characteristics, however both spontaneous rejuvenation and acquisition of age-associated characteristics are seen in a small proportion of cells. (E) Characteristic age distribution of daughter cells, without regard for pairing. In all panels data are expressed as the mean ± the standard deviation. In both conditions, 36 pairs of cells were analyzed from pooled LT-HSC samples obtained from 2 experiments, each using 3 mice.

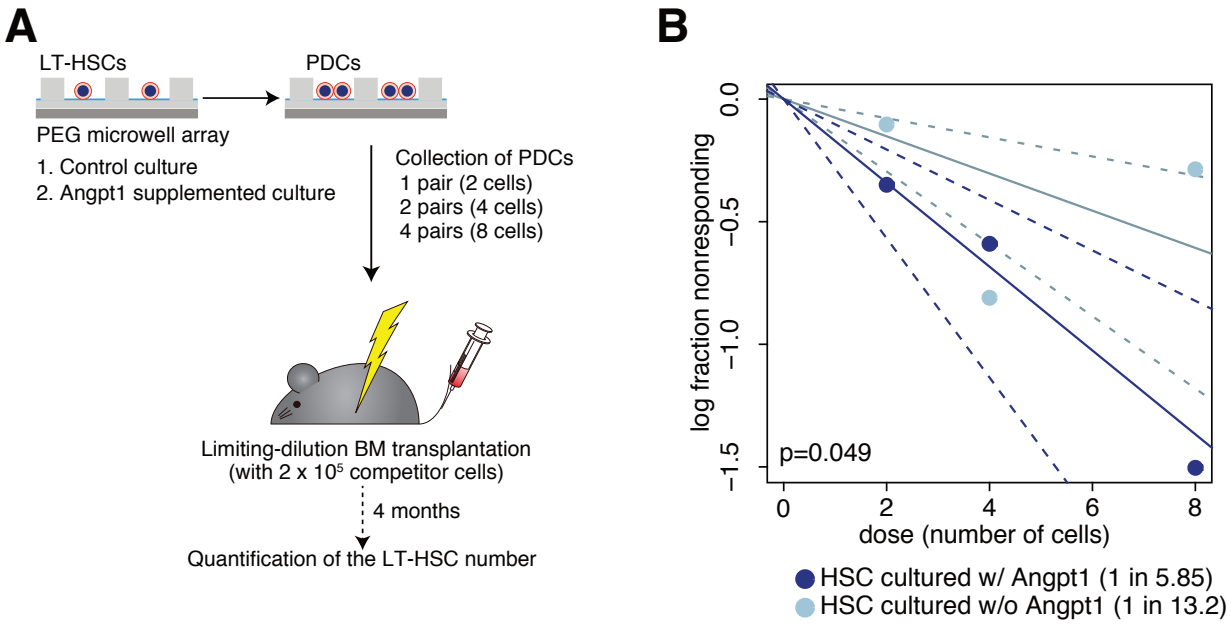

Figure S9. Microwell culture enhances LT-HSC self-renewal. (A) Schematic of limiting dilution bone marrow transplantation (BMT) assay. (B) Limiting dilution BMT of cultured PDCs shows that microwell culture maintains HSC activity *ex vivo* with and without Angpt1 treatment. In all panels data are expressed as the mean ± the standard deviation. Representative data from 2 independent biological replicates are shown. The following number of mice (n) were used: $n = 20$, control 1 pair (2 cells); $n = 9$, control 2 pairs (4 cells); $n = 7$, control 4 pairs (8 cells); $n = 17$, Angpt1 1 pair (2 cells); $n = 9$, Angpt1 2 pairs (4 cells); $n = 9$, Angpt1 4 pairs (8 cells). p-values are determined by extreme value limiting dilution analysis (ELDA) in all panels (Hu & Smyth 2009).

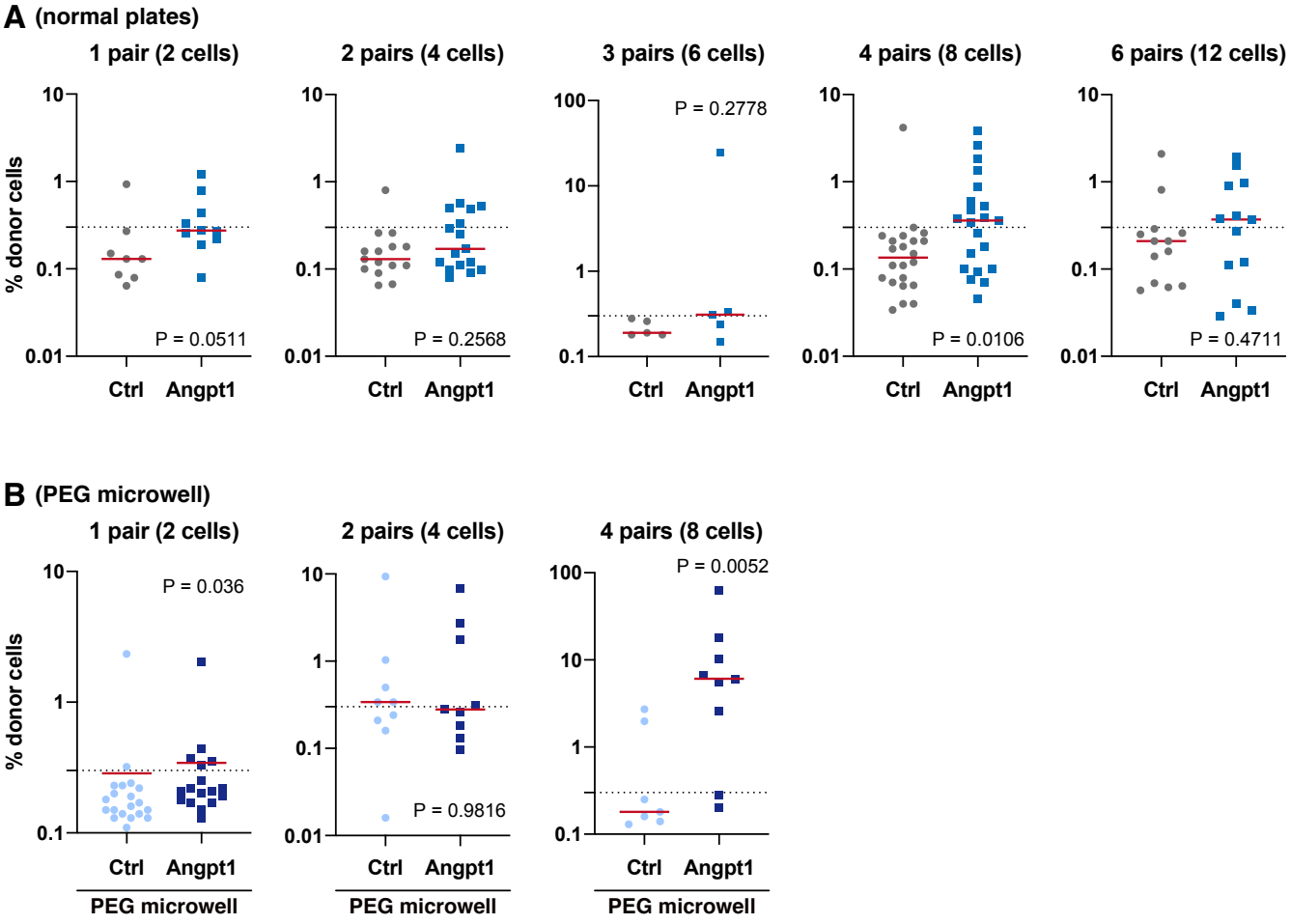

Figure S10. Alternative presentation of bone marrow reconstitution data (related to Figures 3A and S9).
Reconstitution of blood forming activity in irradiated mice via transplantation of pairs of cells derived from LT-HSCs in (A) 96-well plates or (B) micro-well plates. *p*-values are from two-sided t-tests. Horizontal bars indicate mean.

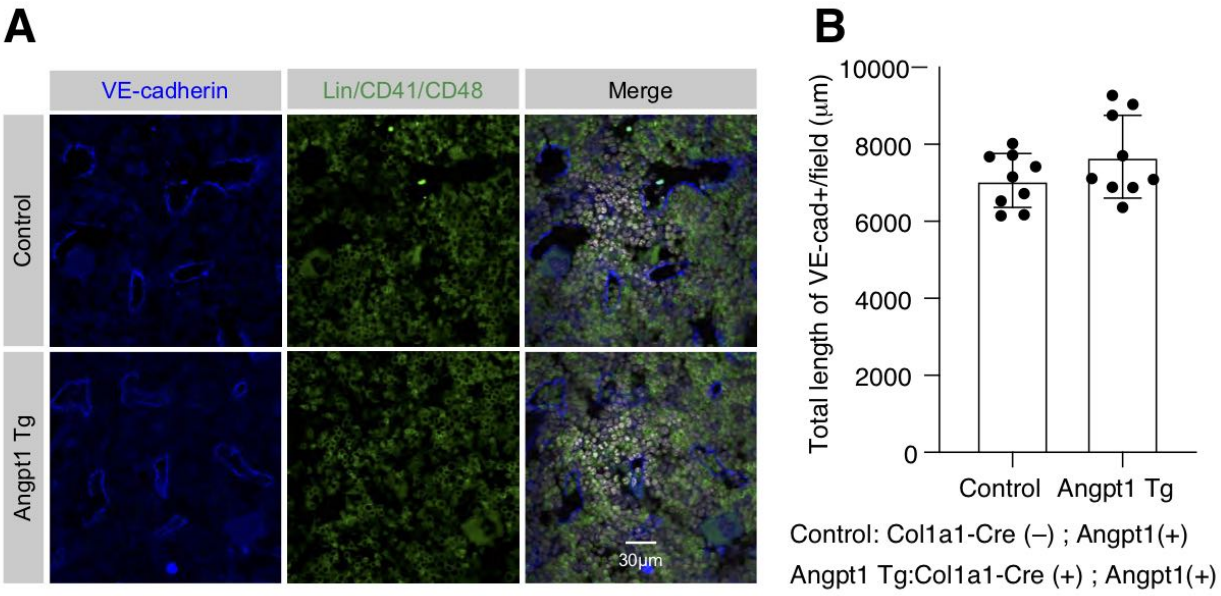

Figure S11. Comparison of vascular length in control and Angpt1 Transgenic mice. (A) Immunohistochemical staining of VE-cadherin (blue) and lineage markers/CD41/CD48 (green). Nuclei are stained with TOTO3 (white). Scale bar is 30μm. (B) Total length of VE-cadherin^{+} vasculature per field. Data are expressed as the mean $\pm$ the standard deviation (control: 154 fields, Angpt1 Tg: 170 fields). Representative data from 3 independent experiments are shown.